nature cell biology

Coordinate control of gene expression noise and interchromosomal interactions in a MAP kinase pathway

Emma McCullagh[1], Anupama Seshan[1,2], Hana El-Samad[1,3] and Hiten D. Madhani[1,3]

In the *Saccharomyces cerevisiae* pheromone-response pathway, the transcription factor Ste12 is inhibited by two mitogen-activated protein (MAP)-kinase-responsive regulators, Dig1 and Dig2. These two related proteins bind to distinct regions of Ste12 but are redundant in their inhibition of Ste12-dependent gene expression. Here we describe three functions for Dig1 that are non-redundant with those of Dig2. First, the removal of Dig1 results in a specific increase in intrinsic and extrinsic noise in the transcriptional outputs of the mating pathway. Second, in *dig1Δ* cells, Ste12 relocalizes from the nucleoplasmic distribution seen in wild-type cells into discrete subnuclear foci. Third, genome-wide insertional chromatin immunoprecipitation studies revealed that Ste12-dependent genes have increased interchromosomal interactions in *dig1Δ* cells. These findings suggest that the regulation of gene expression through long-range gene interactions, a widely observed phenomenon, comes at the cost of increased noise. Consequently, cells may have evolved mechanisms to suppress noise by controlling these interactions.

Cells respond to environmental fluctuations by transducing signals to networks of DNA-binding proteins. Numerous transcriptional regulators, including p53 (ref. 1), E2Fs[2] and Smads[3,4], are subject to overlapping inhibitory mechanisms, yet the logic underlying these potential circuit redundancies remains poorly understood. A well-defined example of such regulatory architecture occurs in the *S. cerevisiae* mating pathway in which the transcription factor Ste12 is inhibited by two MAP kinase (MAPK)-responsive regulators, Dig1 and Dig2. These related proteins are redundant in their suppression of Ste12 activity, because the removal from cells of both proteins is required to derepress pathway activity[5,6]. Despite this redundancy, Dig1 and Dig2 bind to distinct regions of Ste12: Dig1 to the activation domain and Dig2 to the DNA-binding domain[7,8].

Ste12 lies at the terminus of a signal transduction pathway that is initiated by the binding of extracellular pheromones to a G-protein-coupled receptor. This ligand-sensing event triggers the activation of a MAPK cascade, which initiates a cytoplasmic response and transmits the mating signal to the nucleus to activate the transcription factor Ste12 (Fig. 1a). Ste12 regulates the expression of a network of genes whose products are required for the process of mating. Unstimulated cells display a basal level of signalling that increases on stimulation with pheromone. This system has been used recently as a model to measure variability, or noise, in a signal transduction cascade and to ascertain whether such noise is controlled[9,10]. It was found that removal of either of the MAPKs Fus3 or Kss1 did not affect total output variability, suggesting that this natural system may have evolved overlapping mechanisms that buffer against noise[9]. Because the regulation of gene expression noise has been suggested to be important for appropriate input–output responses[11–13], we reasoned that the investigation of noise in the output of the mating pathway might reveal mechanisms that underlie the redundant regulatory architecture controlling Ste12 activity.

RESULTS

Noise in Ste12-dependent gene expression outputs is limited by Dig1

We constructed two Ste12-dependent reporter genes with yellow fluorescent protein (YFP) tags, namely *pAGA1–YFP* and *pFUS1–YFP*. Their output distributions in wild-type and *dig1Δ* cells overlapped less than 5% with the background autofluorescence of yeast (Supplementary Information, Fig. S1). The mean output of *dig1Δ* strains increased 1.4-fold over the wild type, whereas mean fluorescence levels in *dig2Δ* did not change measurably (Fig. 1b), confirming that Dig1 and Dig2 seem redundant in their inhibition of average Ste12-dependent transcription[5,6] when assayed in this manner. As expected, deleting *DIG1* and *DIG2* resulted in a 19-fold and 9-fold increase in mean expression for *pAGA1–YFP* and *pFUS1–YFP*, respectively (Fig. 1b). The mean output of a Ste12-independent green fluorescent protein (GFP)-tagged reporter, *pPMP1–GFP*, was unaffected by the deletion of *DIG1* or *DIG2* (Fig. 1b).

In contrast, examination of the single-cell output distributions of the Ste12-dependent reporters revealed a non-redundant role for Dig1 that is distinct from that of Dig2. Deletion of *DIG1*, but not *DIG2*, significantly increased the variability as measured quantitatively by the coefficient of variation (CV) (Fig. 1c), and qualitatively by the spread

[1]Department of Biochemistry and Biophysics, University of California, San Francisco, 600 16th Street, San Francisco, California 94158, USA. [2]Present address: Department of Biology, Emmanuel College, 400 The Fenway, Boston, Massachusetts 02115, USA.
[3]Correspondence should be addressed to H.D.M. or H.E.-S. (e-mail: hitenmadhani@gmail.com; Hana.El-Samad@ucsf.edu)

Received 22 March 2010; accepted 19 August 2010; published online 19 September 2010; DOI:10.1038/ncb2097

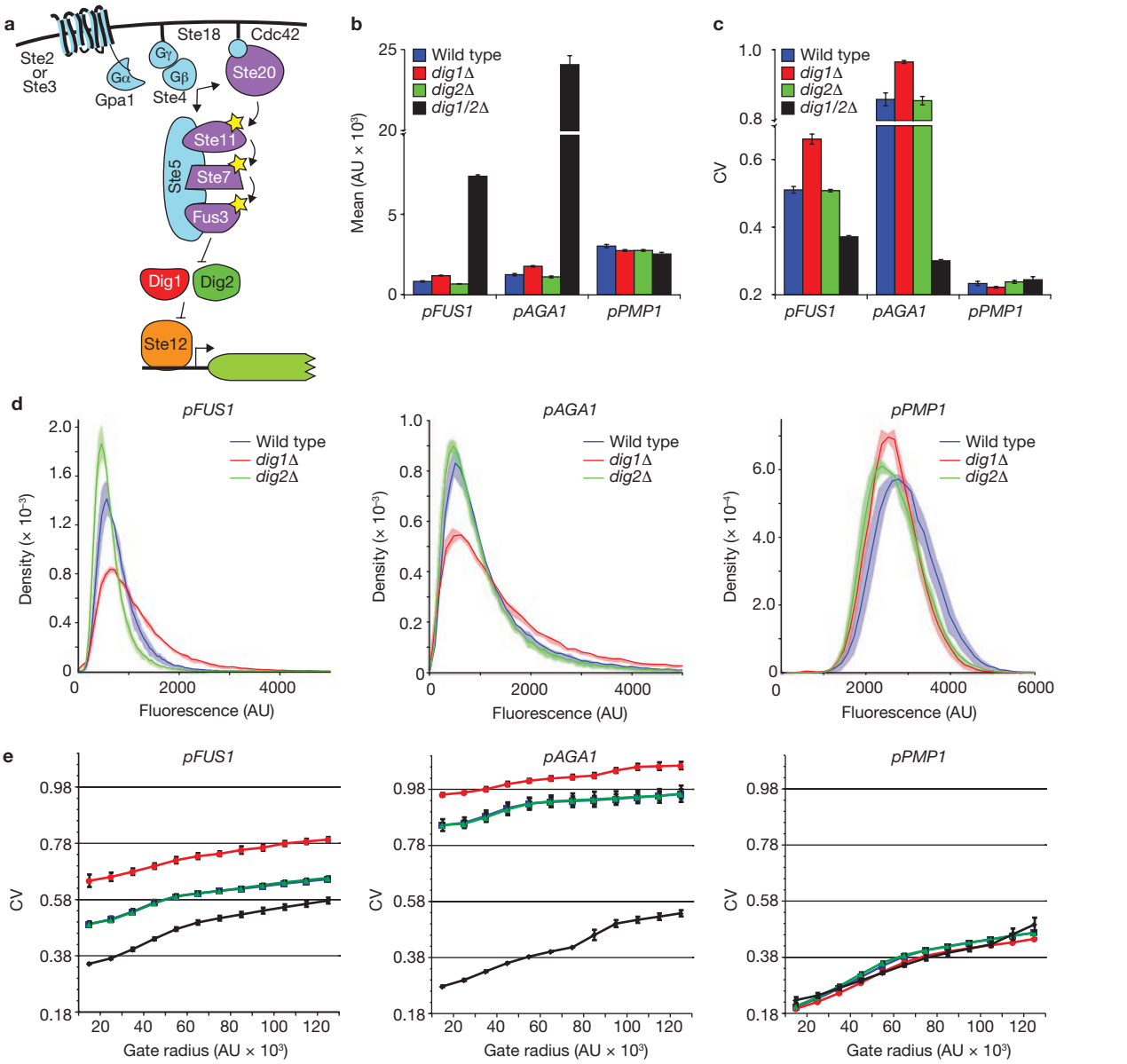

Figure 1 *dig1Δ*, but not *dig2Δ*, cells display increased noise in yeast mating pathway outputs. (**a**) Diagram of the yeast mating MAPK pathway. For simplicity the Ste12 target gene is illustrated as having one Ste12-binding site. (**b**) Mean output for *pFUS1–YFP*, *pAGA1–YFP* and *pPMP1–GFP* in wild-type (blue), *dig1Δ* (red), *dig2Δ* (green) and *dig1Δdig2Δ* (black) mutants in the absence of α-factor. Error bars indicate the s.d. of measurements performed on cell populations from one of three cultures of a given genotype. We refer to these as replicate cultures. The *y* axis is broken between 10,000 and 20,000 AU (arbitrary units). (**c**) Bar graphs illustrating the CV for each strain as in **b**. The *y* axis is broken between 0.7 and 0.8. Student's *t*-test was used to calculate $P = 0.0003$ for the difference between *pAGA1–YFP* and *pAGA1–YFP dig1Δ*, and $P = 0.0014$ for the difference between *pFUS1–YFP* and *pFUS1–YFP dig1Δ*. (**d**) Probability density functions (PDFs) of wild-type (blue), *dig1Δ* (red) and *dig2Δ* (green) for each reporter: *pFUS1–YFP* (left), *pAGA1–YFP* (middle) and *pPMP1–GFP* (right). Solid lines represent the average PDF; the envelope indicates s.d. In **b**–**d**, data shown are for gate 5 (see Methods). (**e**) Plot of CV against gate radius for *pFUS1–YFP* strains (left), *pAGA1–YFP* strains (middle) and *pPMP1–GFP* strains (right). In **b**–**e**, see Methods for gate sizes. Error bars indicate s.d. From each culture, fluorescence values for at least 5,000 cells, and on average between 20,000 and 40,000 cells, were measured.

of the *pAGA1–YFP* and *pFUS1–YFP* distributions (Fig. 1d). The CVs of the *pFUS1–YFP dig1Δ* and *pAGA1–YFP dig1Δ* output distributions were 29.6% ($P = 0.0003$) and 12.5% ($P = 0.0014$) higher, respectively, than those of wild-type and *dig2Δ* (Fig. 1c, d). Cell-sorting experiments indicated that a cell population isolated from the middle of the *dig1Δ* output distribution could regenerate the entire distribution within one or two cell cycles (Fig. 2). Thus, although the steady-state fraction of cells experiencing the high-expression state at any given time point in the *dig1Δ* mutant is modest, the entire population of *dig1Δ* cells is likely to dynamically experience inappropriately high expression states over time. The larger CV of *dig1Δ* output distributions was unexpected, and all the more significant, because the slight increase in mean output in *dig1Δ* cells might be predicted to generate a decrease, rather than an increase, in noise[14]. Furthermore, the increase in noise in *dig1Δ* cell populations was independent of forward scatter and side scatter, which are flow-cytometric surrogate measures of cell size and shape (Fig. 1e; see Methods).

As expected from the increase in mean expression, *dig1Δdig2Δ* double mutants displayed less variability in mating pathway outputs than the wild type (Fig. 1c). The effect of deleting *DIG1* on noise is specific to outputs of the mating pathway, because the deletion of *DIG1* or *DIG2* did not affect the variability in three Ste12-independent reporters, *pPMP1–GFP*, *pYEF3–GFP* and *pAGP1–GFP* (Fig. 1c, d; Supplementary Information, Fig. S2). Furthermore, the changes in noise cannot be due merely to changes in the mean expression or growth rate, because the analysis of several additional mutants illustrate that increased mean output and decreased growth rate do not result in increased noise (Supplementary Information, Fig. S3).

Both intrinsic and extrinsic noise increase in *dig1Δ* cell populations

Gene expression noise can be decomposed into intrinsic and extrinsic components by using a two-colour reporter gene system in which distinct fluorescent proteins are expressed from identical promoters in the same cell[15]. Intrinsic noise is defined as the uncorrelated cell-to-cell variation in levels of these two fluorescent proteins and is thought to reflect stochastic fluctuations in gene expression itself[16–19]. Extrinsic noise is defined as the correlated variation in the levels of the two proteins. Although extrinsic noise is thought to be impacted by cell-to-cell variability in the global cellular state, its origins and effectors are considerably less well understood[9,11,14].

Using a two-colour assay with strains containing GFP and mCherry driven by *pAGA1* (Fig. 3a), we observed that both intrinsic and extrinsic noise increased in *dig1Δ* cell populations in comparison with wild-type and *dig2Δ* cell populations. This result can be seen qualitatively by the decreased density of cells in the centre of the scatter plot of the data for the *dig1*Δ mutant relative to wild-type and *dig2*Δ (Fig. 3b), indicating an increased spread in fluorescence values. Quantitative calculations also reveal increases in the CV measurements (Fig. 3c; Supplementary Information, Fig. S4). The extrinsic noise (η_{ext}) was 22.8% ($P = 0.035$) greater in magnitude in *dig1Δ* cells than in the wild type, whereas the intrinsic noise (η_{int}) was 14.9% ($P = 0.009$) higher in *dig1Δ* cells (Fig. 3c). These patterns of increased intrinsic and extrinsic noise in *dig1Δ* populations were independent of cell size and shape and were specific to Ste12-dependent outputs (Fig. 3d–f; Supplementary Information, Fig. S4d, e).

Dig1 prevents the formation of subnuclear foci of Ste12–GFP molecules

The increased extrinsic noise in *dig1Δ* cell populations could result from the breakdown of a mechanism in which Dig1 limits fluctuations in the levels of the transcription factor Ste12 through an autoregulatory feedback loop at the Ste12 promoter[20–22]. However, this was not the case: replacing the Ste12-dependent Ste12 promoter had no effect on noise (Fig. 4). This posed the possibility that the mechanism by which Dig1 acts on Ste12-dependent genes to limit extrinsic noise is beyond correlations in upstream factors. Extrinsic noise is typically measured by quantifying the correlated variability in the expression from two identical promoters, in this case *pAGA1*. However, more generally, correlated or extrinsic noise in *pAGA1* output would be expected to increase in *dig1Δ* cells if Dig1 limited the correlated expression of all Ste12 outputs in the cell. One way in which this could occur would be if Ste12 target genes co-localized in space in the absence of Dig1. If this were so, the spatial proximity of these genes could increase the dependence of the expression of one Ste12 target gene on the expression of another, perhaps as a result of increased local concentration of activators. For example, if Ste12 target genes were co-localized in space, the induction of one gene could stimulate the induction of a neighbouring Ste12 target gene. Thus, it would be expected that the expression of such co-localized genes would be more correlated, in turn resulting in an increase in extrinsic noise. Given that Ste12 has many known interacting partners and exhibits self-cooperativity[5,6,23–27], Dig1 may function to shield protein–protein interaction domains on Ste12 that would otherwise cause Ste12 to homodimerize or bind to other proteins. The loss of Dig1 might therefore allow DNA-bound Ste12 proteins to enable long-range interchromosomal interactions between Ste12 target genes.

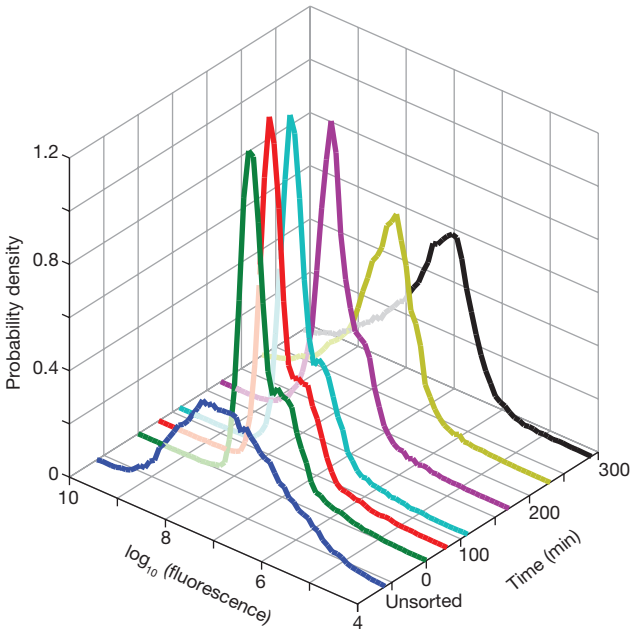

Figure 2 Sorted *dig1Δ* cells can regenerate the entire *pAGA1–YFP* output distribution. *dig1Δ* cells expressing mean levels of *pAGA1–YFP* were sorted and regrown over time. At $t = 0$, 60, 120, 180, 240 and 300 min, cells were removed and the fluorescence distribution was determined ($n = 30{,}000$ cells). Results shown are representative of two independent experiments.

Consistent with this possibility, Ste12–GFP molecules localized to subnuclear foci in *dig1Δ* cells (Fig. 5a, white arrowheads), whereas Ste12–GFP showed granular nucleoplasmic staining in both wild-type and *dig2Δ* cells (Fig. 5a). About 65% of *dig1Δ* cells showed one or more Ste12–GFP foci (Fig. 5b). These foci did not co-localize with the nucleolus (Supplementary Information, Fig. S5a) and focus formation cannot be explained by changes in total Ste12 protein levels because these levels were unaltered in *dig1Δ* and *dig2Δ* cells, as measured by quantitative immunoblotting (Supplementary Information, Fig. S5b). *dig1Δdig2Δ* double mutants also had Ste12–GFP foci, but a slightly higher nucleoplasmic accumulation of Ste12–GFP protein precluded accurate assessment and quantification (Supplementary Information, Fig. S5c). Focus formation in *dig1Δ* cells was specific to Ste12, because the transcription factor Reb1–GFP displayed nucleoplasmic staining in wild-type, *dig1Δ* and *dig2Δ* cells (Fig. 5a).

Focus-suppressing function of Dig1 is not controlled by MAPK signalling

In wild-type cells, stimulation with pheromone does not induce the formation of Ste12–GFP foci (Fig. 5c), indicating that an increase in

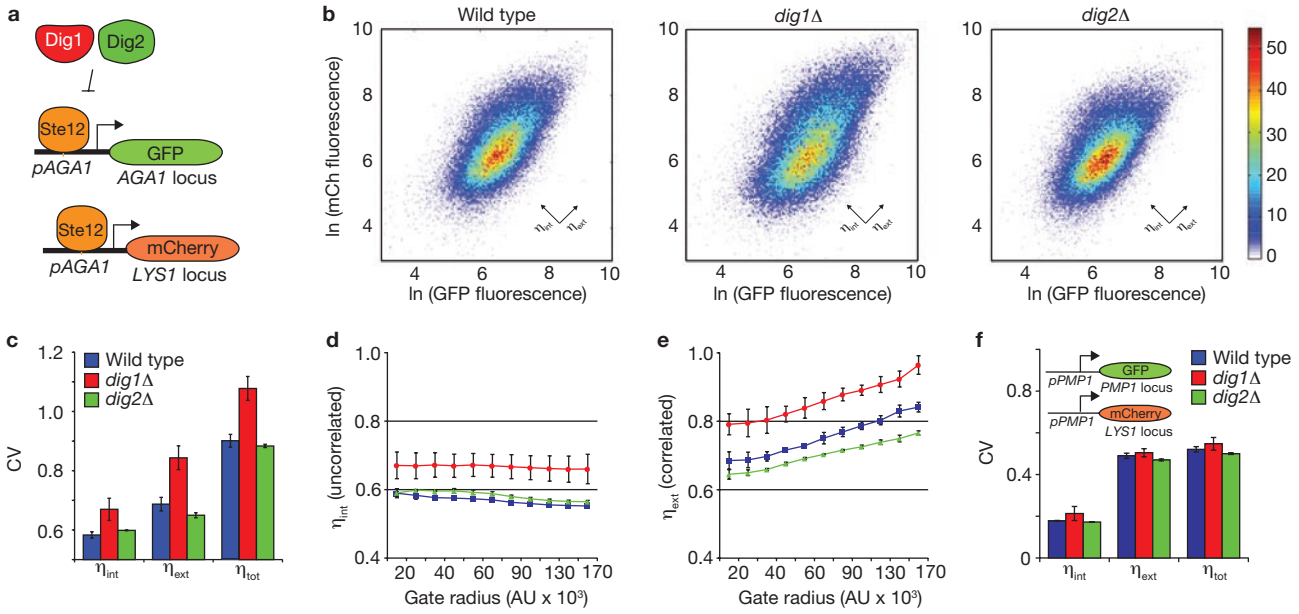

Figure 3 Extrinsic and intrinsic noise in output of mating pathway increase in *dig1Δ* cell populations. (**a**) Diagram of two-colour experiment. *pAGA1–GFP* is in the endogenous *AGA1* locus, whereas *pAGA1–mCherry–AGA1* 3′ untranslated region is inserted into the *LYS1* locus. (**b**) Density plots of wild-type (left), *dig1Δ* (middle) and *dig2Δ* (right). (**c**) Quantification of intrinsic noise (η_{int}), extrinsic noise (η_{ext}) and total noise (η_{tot}) of wild-type (blue), *dig1Δ* (red) and *dig2Δ* (green) populations. Student's *t*-test was used to calculate $P = 0.035$ for increase in intrinsic noise and $P = 0.009$ for increase in extrinsic noise in the *dig1Δ* mutant. Total noise was calculated as $\eta_{tot} = \sqrt{(\eta_{ext} + \eta_{int})}$. (**d**, **e**) Plots of intrinsic (**d**) and extrinsic (**e**) noise against gate radius to control for cell size and shape. (**f**) Quantification of intrinsic, extrinsic and total noise in an Ste12-independent reporter strain in which two fluorophores are driven by *pPMP1* (inset). In **c**–**f** each value is the mean of three replicate cultures and error bars indicate s.d. From each culture, fluorescence values for at least 5,000 cells, and on average between 20,000 and 40,000 cells, were measured.

signalling and transcriptional output is not sufficient to induce their formation. Although it has been suggested that mating signalling inactivates Dig1 (refs 5, 6), we found that this protein remains physically associated with target genes (presumably through Ste12) in cells treated with pheromone (Fig. 5d). Thus, consistent with our finding that Ste12–GFP foci do not form in wild-type cells on stimulation with pheromone, not all activities of Dig1 are eliminated by signalling.

Increased long-range interactions between Ste12 target genes in *dig1Δ* cells

Using a genome-wide adaptation of the single-locus insertional chromatin immunoprecipitation technique[28], we examined interactions between the Ste12 target locus, *pFUS1*, and the rest of the genome in wild-type and *dig1Δ* cells (see Methods). The locus immunoprecipitated efficiently, as seen by the large peak centred on the *FUS1* promoter on the left arm of chromosome III (Fig. 6a). No enrichment was observed at the *pFUS1* locus in the absence of LacI (Supplementary Information, Fig. S6). The 5% of genes (269 genes out of 5,577 total) whose promoters displayed the largest differences in chromatin immunoprecipitation (ChIP)-chip signals between *dig1Δ* cells and wild-type were analysed (Supplementary Information, Table S1). Of the 203 gene regulators for which genome-wide localization data are available[21], only targets of Ste12 and Tec1 displayed a statistically significant increase in interactions with the *FUS1* locus in *dig1Δ* cells (Fig. 6b; similar results were obtained for 1%, 3% and 10% cutoffs). Moreover, these physical interactions were dependent on the presence of Ste12 (Fig. 6c; Supplementary Information, Table S1). Tec1 and Ste12 are known to interact and are found at promoters of genes involved in both mating and filamentous growth[22,27]. Well-studied genes implicated in these processes were featured prominently among those that displayed increased physical interactions with the *FUS1* locus in *dig1Δ* cells (Fig. 6d). We constructed promoter–YFP fusions for 11 of these Ste12 target genes and found that the mean expression increased for seven of them on deletion of *DIG1* (Supplementary Information, Fig. S7a). Rigorous analysis of the changes in noise for these genes is complicated by the fact that the means increase significantly and the relationships between the means and CVs are unknown. However, we note that the removal of Dig1 induces a broadening of the output distributions that is highly reminiscent of trends seen with the *pFUS1–YFP* and *pAGA1–YFP* reporter strains (Supplementary Information, Fig. S7b).

Non-redundant roles for Dig1 in growth, mating, and gene induction kinetics

Under basal conditions, the mating pathway must appropriately balance the level of signalling to avoid cell cycle arrest and mating projection formation induced by pathway activation with a requirement for maintaining basal signalling to express key pathway components[29]. This balance might be expected to be disrupted in *dig1Δ* cells, with repercussions for growth under basal conditions and mating in the presence of a pheromone signal. Therefore, cell-to-cell variability in outputs of the mating pathway could influence fitness. We found that *dig1Δ* cells grow more poorly than wild-type or *dig2Δ* cells and that this defect is rescued by the deletion of *STE12* (Fig. 7a, b). In addition, *dig1Δ* cells show a kinetic defect in cell–cell fusion compared to wild-type and *dig2Δ* cells, as measured quantitatively with a fluorescent-based assay in which the accumulation of double-positive fluorescent cells was scored (Fig. 7c–e; Supplementary Information, Fig. S8; see

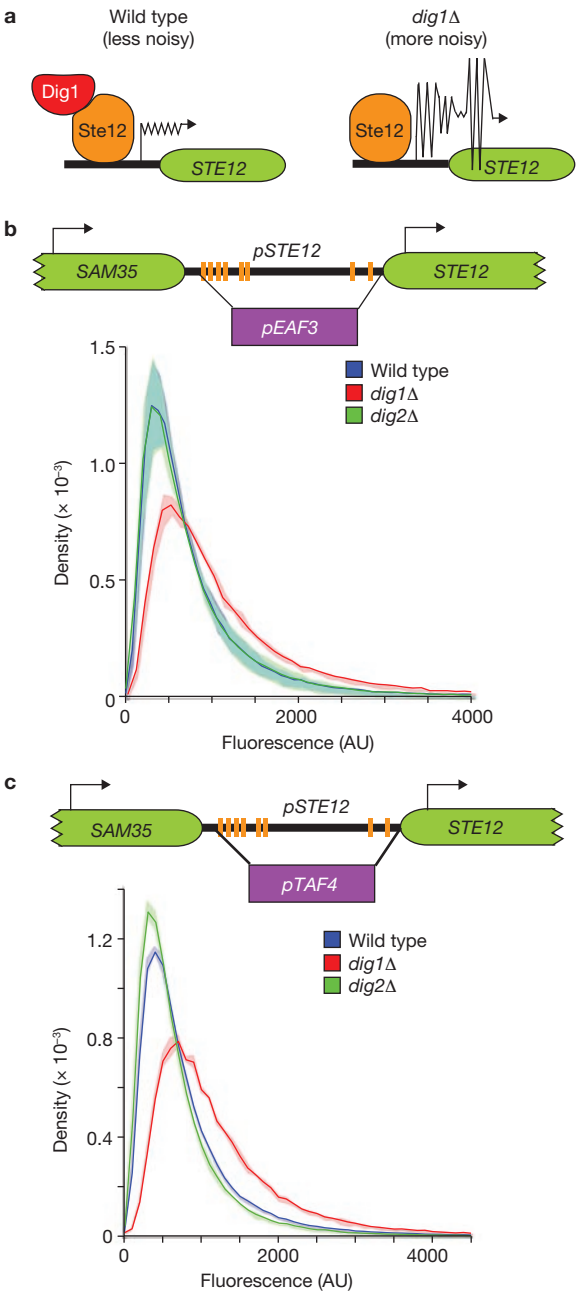

Figure 4 Increased noise in mating pathway outputs in *dig1Δ* cells is not due to feedback at the *STE12* promoter. (**a**) Model for the increased noise in the mating pathway in *dig1Δ* cells. (**b**) Top: *pSTE12* was replaced with the Ste12-independent promoter *pEAF3*. Bottom: PDFs of *pAGA1–YFP* strains containing *pEAF3–STE12*. (**c**) Top: *pSTE12* was replaced with the Ste12-independent promoter *pTAF4*. Bottom: PDFs of *pAGA1–YFP* strains containing *pTAF4–STE12*. In **b** and **c** the wild type is shown in blue, *dig1Δ* in red and *dig2Δ* in green. The mean PDF of three replicate cultures is shown in the solid line, and the envelope indicates s.d. From each culture, fluorescence values for at least 5,000 cells, and on average between 20,000 and 40,000 cells, were measured.

Methods). This defect is unlikely to be due to the slight increase in mean pathway output in *dig1Δ* cells, because previous studies found that even large increases in basal signalling do not decrease mating efficiency[30]. The defect in fusion between mating partners is mirrored by two quantitative changes in the induction of pheromone-inducible genes in *dig1Δ* cells (Fig. 8a). First, a larger proportion of *dig1Δ* cells do not induce *pAGA1–YFP* or *pFUS1–YFP* reporter genes in response to pheromone treatment (Fig. 8b). Second, the population of *dig1Δ* cells that does respond to pheromone shows a decreased dynamic range in the induction of pheromone-inducible gene expression (Fig. 8c).

DISCUSSION

Recent work has shown that *DIG1* and *DIG2* were derived from a single parental gene that existed before the whole-genome duplication (WGD) that occurred in the ancestor of *S. cerevisiae* 100–200 million years ago[31]. Their continued presence in the genome suggests that their maintenance has an adaptive role. Indeed, previous work indicates that Dig1 and Dig2 inhibit Ste12 by interacting with distinct domains of the transcription factor, implying biochemical specialization[7,8]. However, their genetic redundancy for inhibiting Ste12 was puzzling. Studies presented here revealed three functions of Dig1 that are not redundant with those of Dig2: first, control of gene expression noise, second, regulation of the intranuclear distribution of Ste12, and third, the control of long-range interactions between Ste12 target genes. We discuss below how these three functions may be related and the broader implications of these findings.

Dig1 is a well-studied regulatory protein that functions specifically in the pheromone response pathway and has only one reported biochemical function: to bind to a domain of Ste12 involved in protein–protein interactions[5–8,32,33]. The loss of Dig1 is therefore expected solely to unshield protein–protein interaction domains on the Ste12 transcription factor. Although indirect mechanisms are always difficult to rule out, we propose that this unshielding induces aggregation of Ste12 molecules and target genes, which results in increased cell-to-cell variability in the basal output of the pheromone response pathway. Dig2, which binds the distinct DNA-binding domain of Ste12 (refs 7, 8), does not share these functions. The aggregation of Ste12 molecules into one or two foci may create a domain within the nucleus where the transcription of Ste12 target genes can be activated. Our model suggests that the transcription of Ste12 target genes within the focus is more coordinated such that if one gene in the focus is transcribed, the others are, in turn, more likely to be expressed. Thus, such correlated expression within a single cell would be expected to yield increased correlated cell-to-cell variability in the transcriptional output of the pathway.

Transcriptional regulation that involves looping of DNA between distant sites by means of protein–protein interactions has been observed for the *lac* operon[34–38] and λ phage[39,40]. In the context of the results described here, it is notable that computational models of the *lac* system suggest that gene regulation by DNA looping can affect fluctuations in transcription[41]. These models predict that, for transcriptional activators, DNA looping should increase noise in transcriptional outputs. Our model for the function of Dig1 is consistent with these theoretical predictions.

Recently, interchromosomal and intrachromosomal interactions have been detected in other systems[42–45]. In erythroid cells, for example, Klf1-regulated genes, including *Hba* and *Hbb* globin genes, display long-range interchromosomal and intrachromosomal interactions[42]. Although these interactions tend to correlate with transcriptional regulation and sites of active transcription, their precise functions remain a matter of considerable debate. Our observations suggest that although these long-range interactions could be important for gene expression, they may come at the cost of increased variability. This notion is in concordance with an emerging view that, in some cases, these gene interactions can be deleterious and

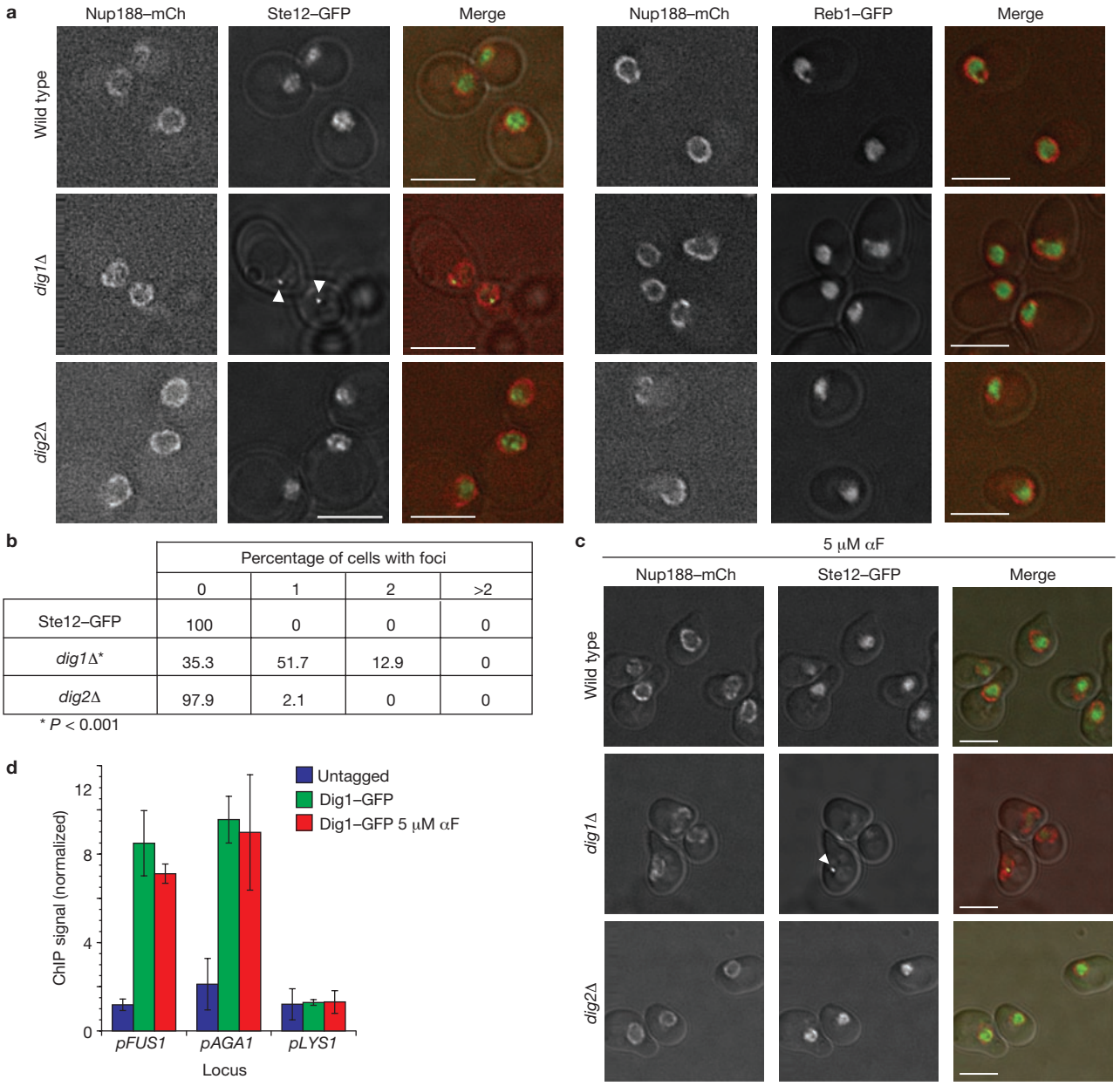

Figure 5 Ste12–GFP forms nuclear foci in *dig1Δ* cells. (**a**) Fluorescence microscopy images of Ste12–GFP/Nup188–mCherry (left) and Reb1–GFP/Nup188–mCherry (right). Ste12–GFP forms nuclear foci in *dig1Δ* (white arrowheads). (**b**) Quantification of foci seen in **a**; $n = 100$ (wild type), $n = 116$ (*dig1Δ*), $n = 95$ (*dig2Δ*). Distributions of foci in all mutants were compared with the wild type by the χ^2 test; only the distribution of foci in *dig1Δ* was statistically significant ($P < 0.001$). The quantification shown is representative of two independent experiments. (**c**) Ste12–GFP localization on addition of 5 μM α-factor (αF) for 1 h. (**d**) Normalized ChIP signal of Dig1–GFP at *AGA1*, *FUS1* and *LYS1* promoters in the absence and presence of 5 μM pheromone. Error bars indicate s.d. for three independent immunoprecipiations. Scale bars, 5 μm.

even mutagenic[46]. It will be interesting to explore whether mechanisms of noise regulation are pervasive among regulatory circuits that involve long-range DNA interactions and the extent to which gene localization is balanced with a need for limiting noise.

Although establishing the generality of the effect of aggregate formation on output variability will require further investigation, we note that subcellular protein and DNA aggregation is not uncommon in biology. DNA replication and gene activation can occur in 'factories' located at the nuclear periphery[47–51]. Sites of DNA damage along with proteins that respond to DNA damage form nuclear foci in yeast[52,53]. Telomeres are also known to cluster in the nucleus[54]. Cytoplasmic P-bodies are foci of proteins involved in messenger RNA degradation and translational inhibition[55–57]. Given our data, these foci may serve, in some cases, to promote simultaneity in cellular transactions. The development of assays that can distinguish between correlated and uncorrelated noise in these systems would allow the testing of such concepts. □

METHODS

Methods and any associated references are available in the online version of the paper at http://www.nature.com/naturecellbiology/

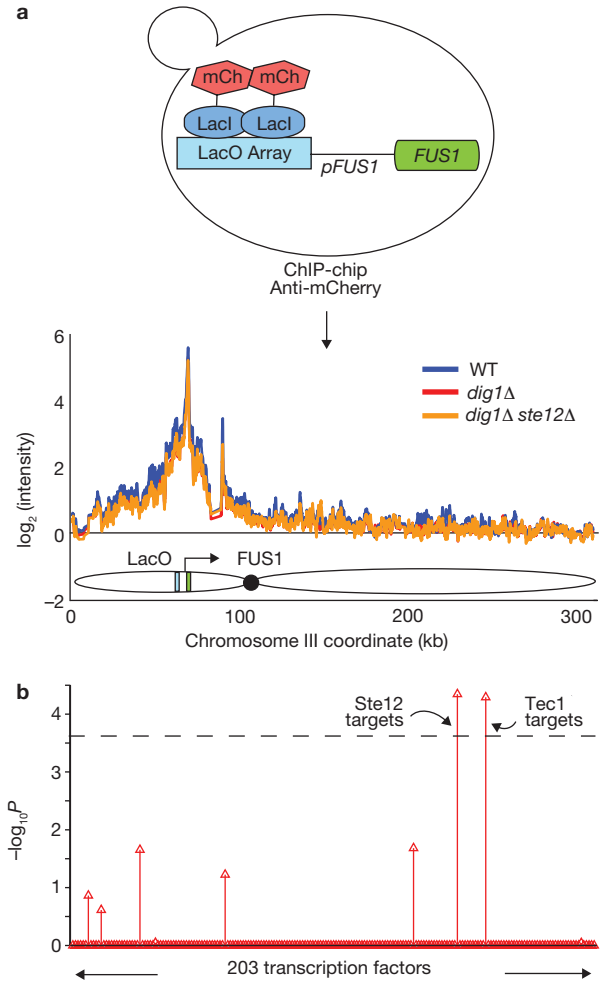

c

Transcription factor	Hypergeometric *P*	
	dig1Δ/WT	*dig1Δste12Δ*/WT
Ste12	4.52×10^{-5}	1.0
Tec1	5.12×10^{-5}	1.0

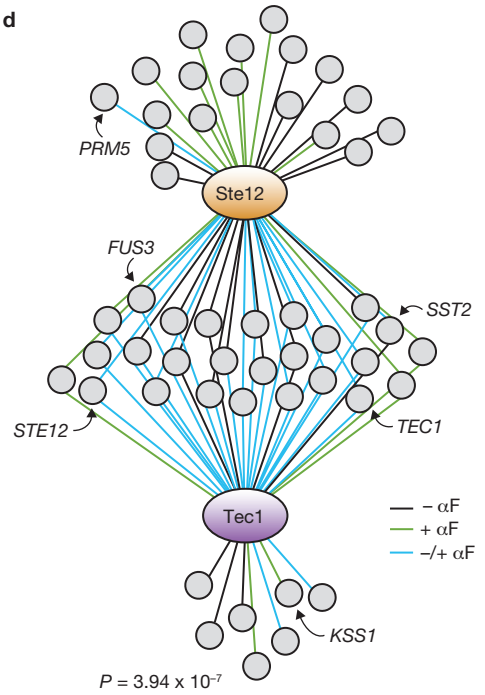

Figure 6 ChIP-chip of Ste12 target locus reveals long-range interactions with other Ste12 target genes. (**a**) Top: experimental set-up. LacI–mCherry was immunoprecipitated from cells and the *FUS1* locus (green), marked with an array of Lac operators (light blue), was efficiently pulled down (see peaks centred on Lac operators in graph below) in wild-type (blue), *dig1Δ* (red) and *dig1Δste12Δ* (orange) cells. Bottom: graph illustrating the ChIP-chip signal along chromosome III, where the array of Lac operators is inserted. See Methods for experimental details. (**b**) Difference maps were calculated and genes were ordered by increasing median value of the region spanning –500 base pairs (bp) to 0 bp, with respect to the translation start site. The top 5% of differences (269 genes; Supplementary Information, Table S1) were analysed for enrichment of target genes of 203 transcription factors[21]. The dashed line indicates the Bonferroni-corrected *P* value of 0.05. (**c**) Bonferroni-corrected *P* values for enrichment of Ste12 and Tec1 target genes in the top 5% of genes with the greatest differences in *dig1Δ* versus wild-type and *dig1Δste12Δ* versus wild-type (Supplementary Information, Table S1). (**d**) Ste12 and Tec1 target genes (in the presence and absence of pheromone[21]) found in the list of 5% of genes with the largest differences in *dig1Δ* versus wild-type data sets. *P* values were calculated by hypergeometric testing.

Note: Supplementary Information is available on the Nature Cell Biology website.

ACKNOWLEDGEMENTS

We thank J. S. Weissman, E. K. O'Shea, J. E. Haber, W. A. Lim, A. D. Johnson and D. J. Sherratt for plasmids and protocols; C. D. Chun and P. D. Hartley for help in conducting and analysing the ChIP-chip experiments; W. F. Marshall and K. Wemmer for assistance with microscopy; and A. D. Johnson, S. Komili, W. F. Marshall and S. Shankar for helpful comments on the manuscript. This work was supported by a Genentech Fellowship and a National Science Foundation Predoctoral Fellowship to E.M., a National Institutes of Health (NIH) Ruth L. Kirschstein National Research Service Award to A.S., and funding from the University of California, San Francisco, Program for Breakthrough Biomedical Research and a NIH grant (R01 GM086379) to H.D.M. and H.E.-S.

AUTHOR CONTRIBUTIONS

E.M. constructed all strains and performed and analysed all experiments except the fluorescence-activated cell sorting (FACS)-based mating assay. A.S. constructed strains for and performed the FACS-based mating assay. H.E.-S. and E.M. wrote custom MATLAB software and conducted data analyses for the FACS assays. E.M., H. E.-S. and H.D.M. wrote the manuscript.

COMPETING FINANCIAL INTERESTS

The authors declare no competing financial interests.

Published online at http://www.nature.com/naturecellbiology
Reprints and permissions information is available online at http://npg.nature.com/reprintsandpermissions/

1. Marine, J. C. *et al.* Keeping p53 in check: essential and synergistic functions of Mdm2 and Mdm4. *Cell Death Differ.* **13,** 927–934 (2006).
2. DeGregori, J. & Johnson, D. G. Distinct and overlapping roles for E2F family members in transcription, proliferation and apoptosis. *Curr. Mol. Med.* **6,** 739–748 (2006).
3. Moustakas, A. & Heldin, C. H. The regulation of TGFβ signal transduction. *Development* **136,** 3699–3714 (2009).
4. Xu, L. Regulation of Smad activities. *Biochim. Biophys. Acta* **1759,** 503–513 (2006).
5. Tedford, K., Kim, S., Sa, D., Stevens, K. & Tyers, M. Regulation of the mating pheromone and invasive growth responses in yeast by two MAP kinase substrates. *Curr. Biol.* **7,** 228–238 (1997).
6. Cook, J. G., Bardwell, L., Kron, S. J. & Thorner, J. Two novel targets of the MAP kinase Kss1 are negative regulators of invasive growth in the yeast *Saccharomyces cerevisiae*. *Genes Dev.* **10,** 2831–2848 (1996).

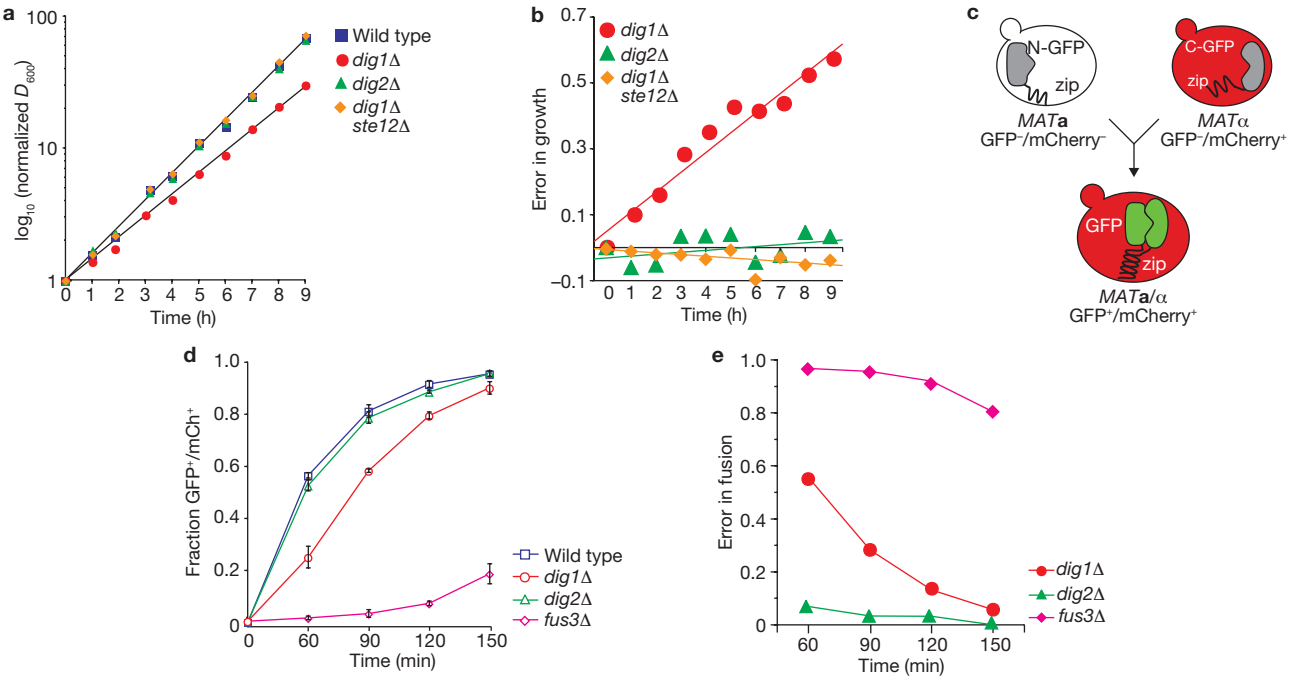

Figure 7 *dig1Δ* cells display defects in growth and cell-cell fusion. (**a**) Exponential-phase wild-type (blue squares), *dig1Δ* (red circles), *dig2Δ* (green triangles) and *dig1Δste12Δ* (orange diamonds) cells were grown for 9 h, and attenuance at 600 nm (D_{600}) was measured hourly. Data shown are representative of four independent experiments. (**b**) Error in growth. D_{600} of mutants (*dig1Δ* in red, *dig2Δ* in green and *dig1Δste12Δ* in orange) was compared with that of the wild type by calculation from the equation $1 - [D_{600}(\text{mutant})]/D_{600}(\text{wild type})]$. (**c**) Diagram for FACS-based cell fusion assay. See Methods for details. (**d**) Fraction of GFP$^+$/mCherry$^+$ cells over time for wild type (blue), *dig1Δ* (red), *dig2Δ* (green) and *fus3Δ* (pink). Samples were analysed at 0, 60, 90, 120 and 150 min. Error bars indicate s.d. for three independent experiments. In each independent experiment, between 3,000 and 10,000 cells were analysed. (**e**) Cell–cell fusion error for mutants (*dig1Δ* in red, *dig2Δ* in green and *fus3Δ* in pink) was calculated in from the equation $1 - [(\text{fraction of mutant fused})/(\text{fraction of wild type fused})]$.

7. Bardwell, L., Cook, J. G., Zhu-Shimoni, J. X., Voora, D. & Thorner, J. Differential regulation of transcription: repression by unactivated mitogen-activated protein kinase Kss1 requires the Dig1 and Dig2 proteins. *Proc. Natl Acad. Sci. USA* **95,** 15400–15405 (1998).
8. Olson, K. A. *et al.* Two regulators of Ste12p inhibit pheromone-responsive transcription by separate mechanisms. *Mol. Cell. Biol.* **20,** 4199–4209 (2000).
9. Colman-Lerner, A. *et al.* Regulated cell-to-cell variation in a cell-fate decision system. *Nature* **437,** 699–706 (2005).
10. Yu, R. C. *et al.* Negative feedback that improves information transmission in yeast signalling. *Nature* **456,** 755–761 (2008).
11. Newman, J. R. *et al.* Single-cell proteomic analysis of *S. cerevisiae* reveals the architecture of biological noise. *Nature* **441,** 840–846 (2006).
12. Cagatay, T., Turcotte, M., Elowitz, M. B., Garcia-Ojalvo, J. & Suel, G. M. Architecture-dependent noise discriminates functionally analogous differentiation circuits. *Cell* **139,** 512–522 (2009).
13. Bollenbach, T. *et al.* Precision of the Dpp gradient. *Development* **135,** 1137–1146 (2008).
14. Volfson, D. *et al.* Origins of extrinsic variability in eukaryotic gene expression. *Nature* **439,** 861–864 (2006).
15. Elowitz, M. B., Levine, A. J., Siggia, E. D. & Swain, P. S. Stochastic gene expression in a single cell. *Science* **297,** 1183–1186 (2002).
16. McAdams, H. H. & Arkin, A. Stochastic mechanisms in gene expression. *Proc. Natl Acad. Sci. USA* **94,** 814–819 (1997).
17. Becskei, A., Kaufmann, B. B. & van Oudenaarden, A. Contributions of low molecule number and chromosomal positioning to stochastic gene expression. *Nat. Genet.* **37,** 937–944 (2005).
18. Raser, J. M. & O'Shea, E. K. Control of stochasticity in eukaryotic gene expression. *Science* **304,** 1811–1814 (2004).
19. Blake, W. J., KÆrn, M., Cantor, C. R. & Collins, J. J. Noise in eukaryotic gene expression. *Nature* **422,** 633–637 (2003).
20. Ren, B. *et al.* Genome-wide location and function of DNA binding proteins. *Science* **290,** 2306–2309 (2000).
21. Harbison, C. T. *et al.* Transcriptional regulatory code of a eukaryotic genome. *Nature* **431,** 99–104 (2004).
22. Zeitlinger, J. *et al.* Program-specific distribution of a transcription factor dependent on partner transcription factor and MAPK signaling. *Cell* **113,** 395–404 (2003).
23. Dolan, J. W. & Fields, S. Overproduction of the yeast STE12 protein leads to constitutive transcriptional induction. *Genes Dev.* **4,** 492–502 (1990).
24. Yuan, Y. L. & Fields, S. Properties of the DNA-binding domain of the *Saccharomyces cerevisiae* STE12 protein. *Mol. Cell. Biol.* **11,** 5910–5918 (1991).
25. Baur, M., Esch, R. K. & Errede, B. Cooperative binding interactions required for function of the Ty1 sterile responsive element. *Mol. Cell. Biol.* **17,** 4330–4337 (1997).
26. Errede, B. & Ammerer, G. STE12, a protein involved in cell-type-specific transcription and signal transduction in yeast, is part of protein–DNA complexes. *Genes Dev.* **3,** 1349–1361 (1989).
27. Madhani, H. D. & Fink, G. R. Combinatorial control required for the specificity of yeast MAPK signaling. *Science* **275,** 1314–1317 (1997).
28. Hoshino, A. & Fujii, H. Insertional chromatin immunoprecipitation: a method for isolating specific genomic regions. *J. Biosci. Bioeng.* **108,** 446–449 (2009).
29. Fields, S., Chaleff, D. T. & Sprague, G. F., Jr. Yeast *STE7*, *STE11*, and *STE12* genes are required for expression of cell-type-specific genes. *Mol. Cell. Biol.* **8,** 551–556 (1988).
30. Stevenson, B. J., Rhodes, N., Errede, B. & Sprague, G. F. Jr. Constitutive mutants of the protein kinase STE11 activate the yeast pheromone response pathway in the absence of the G protein. *Genes Dev.* **6,** 1293–1304 (1992).
31. Gordon, J. L., Byrne, K. P. & Wolfe, K. H. Additions, losses, and rearrangements on the evolutionary route from a reconstructed ancestor to the modern *Saccharomyces cerevisiae* genome. *PLoS Genet.* **5,** e1000485 (2009).
32. Pi, H., Chien, C. T. & Fields, S. Transcriptional activation upon pheromone stimulation mediated by a small domain of *Saccharomyces cerevisiae* Ste12p. *Mol. Cell. Biol.* **17,** 6410–6418 (1997).
33. Chou, S., Lane, S. & Liu, H. Regulation of mating and filamentation genes by two distinct Ste12 complexes in *Saccharomyces cerevisiae*. *Mol. Cell. Biol.* **26,** 4794–4805 (2006).
34. Kramer, H. *et al.* lac repressor forms loops with linear DNA carrying two suitably spaced lac operators. *EMBO J.* **6,** 1481–1491 (1987).
35. Whitson, P. A., Hsieh, W. T., Wells, R. D. & Matthews, K. S. Influence of supercoiling and sequence context on operator DNA binding with *lac* repressor. *J. Biol. Chem.* **262,** 14592–14599 (1987).
36. Whitson, P. A., Hsieh, W. T., Wells, R. D. & Matthews, K. S. Supercoiling facilitates *lac* operator-repressor-pseudooperator interactions. *J. Biol. Chem.* **262,** 4943–4946 (1987).
37. Eismann, E., von Wilcken-Bergmann, B. & Muller-Hill, B. Specific destruction of the second lac operator decreases repression of the lac operon in *Escherichia coli* fivefold. *J. Mol. Biol.* **195,** 949–952 (1987).
38. Mossing, M. C. & Record, M. T., Jr. Thermodynamic origins of specificity in the *lac* repressor-operator interaction. Adaptability in the recognition of mutant operator sites. *J. Mol. Biol.* **186,** 295–305 (1985).

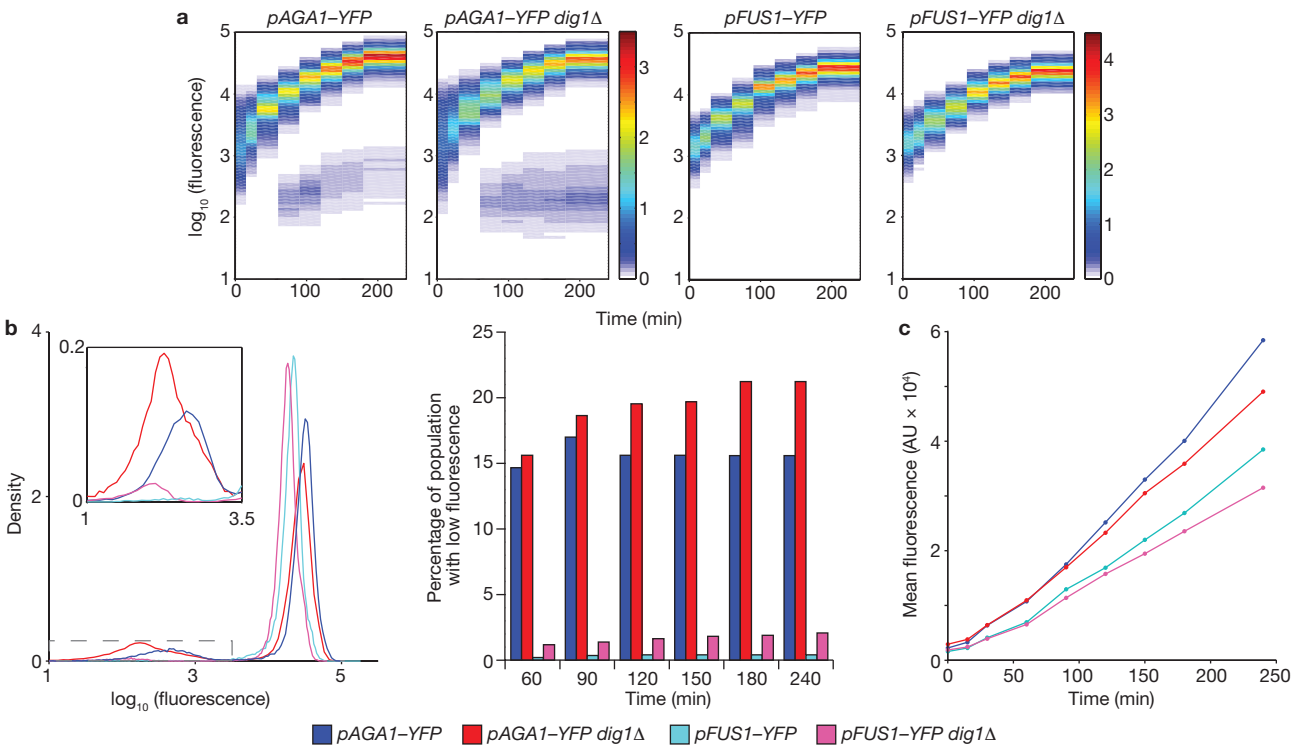

Figure 8 Time course of induction of *pAGA1–YFP* and *pFUS1–YFP* after treatment with pheromone. (**a**) Heat map of induction of *pAGA1–YFP* (left) and *pFUS1–YFP* (right) in wild-type and *dig1Δ* cells. Samples were analysed at 0, 15, 30, 60, 90, 120, 150, 180 and 240 min. (**b**) Left: probability density functions for the 150-min time point of *pAGA1–YFP* (dark blue), *pAGA1–YFP dig1Δ* (dark red), *pFUS1–YFP* (light blue) and *pFUS1–YFP dig1Δ* (pink). The inset is an enlargement of the area marked by the grey-dashed line. Right: plot of the percentage of cells in the low fluorescence population against time. (**c**) Plot of the mean fluorescence of the transcriptionally induced populations in **a** against time. Transcriptionally induced and uninduced populations (see **a**) were separated, and the means of the high-expressing populations were calculated for each time point. The colours are as in **b**. Data shown are representative of three independent experiments. For each time point, fluorescence values for at least 5,000 cells, and on average between 20,000 and 40,000 cells, were measured.

39. Dodd, I. B., Perkins, A. J., Tsemitsidis, D. & Egan, J. B. Octamerization of λ CI repressor is needed for effective repression of P_{RM} and efficient switching from lysogeny. *Genes Dev.* **15,** 3013–3022 (2001).
40. Revet, B., von Wilcken-Bergmann, B., Bessert, H., Barker, A. & Muller-Hill, B. Four dimers of λ repressor bound to two suitably spaced pairs of λ operators form octamers and DNA loops over large distances. *Curr. Biol.* **9,** 151–154 (1999).
41. Vilar, J. M. & Leibler, S. DNA looping and physical constraints on transcription regulation. *J. Mol. Biol.* **331,** 981–989 (2003).
42. Schoenfelder, S. *et al.* Preferential associations between co-regulated genes reveal a transcriptional interactome in erythroid cells. *Nat. Genet.* **42,** 53–61 (2009).
43. Spilianakis, C. G., Lalioti, M. D., Town, T., Lee, G. R. & Flavell, R. A. Interchromosomal associations between alternatively expressed loci. *Nature* **435,** 637–645 (2005).
44. Zhao, Z. *et al.* Circular chromosome conformation capture (4C) uncovers extensive networks of epigenetically regulated intra- and interchromosomal interactions. *Nat. Genet.* **38,** 1341–1347 (2006).
45. Apostolou, E. & Thanos, D. Virus infection induces NF-κB-dependent interchromosomal associations mediating monoallelic IFN-β gene expression. *Cell* **134,** 85–96 (2008).
46. Lin, C. *et al.* Nuclear receptor-induced chromosomal proximity and DNA breaks underlie specific translocations in cancer. *Cell* **139,** 1069–1083 (2009).
47. Brickner, J. H. & Walter, P. Gene recruitment of the activated *INO1* locus to the nuclear membrane. *PLoS Biol.* **2,** e342 (2004).
48. Kitamura, E., Blow, J. J. & Tanaka, T. U. Live-cell imaging reveals replication of individual replicons in eukaryotic replication factories. *Cell* **125,** 1297–1308 (2006).
49. Meister, P., Taddei, A. & Gasser, S. M. In and out of the replication factory. *Cell* **125,** 1233–1235 (2006).
50. Taddei, A. *et al.* Nuclear pore association confers optimal expression levels for an inducible yeast gene. *Nature* **441,** 774–778 (2006).
51. Branco, M. R. & Pombo, A. Intermingling of chromosome territories in interphase suggests role in translocations and transcription-dependent associations. *PLoS Biol.* **4,** e138 (2006).
52. Lisby, M., Mortensen, U. H. & Rothstein, R. Colocalization of multiple DNA double-strand breaks at a single Rad52 repair centre. *Nat. Cell Biol.* **5,** 572–577 (2003).
53. Bishop, D. K. RecA homologs Dmc1 and Rad51 interact to form multiple nuclear complexes prior to meiotic chromosome synapsis. *Cell* **79,** 1081–1092 (1994).
54. Cockell, M. & Gasser, S. M. Nuclear compartments and gene regulation. *Curr. Opin. Genet. Dev.* **9,** 199–205 (1999).
55. Parker, R. & Sheth, U. P bodies and the control of mRNA translation and degradation. *Mol. Cell* **25,** 635–646 (2007).
56. Sheth, U. & Parker, R. Decapping and decay of messenger RNA occur in cytoplasmic processing bodies. *Science* **300,** 805–808 (2003).
57. Cougot, N., Babajko, S. & Seraphin, B. Cytoplasmic foci are sites of mRNA decay in human cells. *J. Cell Biol.* **165,** 31–40 (2004).

METHODS

Strains. All yeast strains used are derived from BY4743, of the s288c background, and are described in Supplementary Information, Table S2. Yeast knockouts were generated by conventional lithium acetate and poly(ethylene glycol) procedures. YFP, eGFP (from pFA6a–EGFP–HIS3MX) and mCherry (from pFA6a–mCherry–HIS3MX or pFA6a–GFPtomCherry–URA3MX from J. S. Weissman) reporters for the mating pathway were constructed by using methods as described[58], and *pPMP1*-fluorophore fusions were constructed using plasmids pFA6a–EGFP–HIS3MX6 and pFA6a–GFPtomCherry–URA3MX.

Growth and fluorescence measurements by flow cytometry. Cells were grown in 1-ml cultures for 36 h in 96-well deep-pocket plates (Costar). D_{600} measurements were taken and cultures were diluted to $D_{600} = 0.08$ and grown for 10 h. A Becton Dickinson LSR-II flow cytometer was used, along with an autosampler device (HTS) controlled by custom software, to collect data over a sampling time of 7 s (ref. 11). YFP and GFP were excited at 488 nm and fluorescence was collected through a 505-nm long-pass filter and HQ530/30 and HQ515/20 bandpass filters (Chroma Technology), respectively. mCherry was excited at 532 nm and fluorescence collected through a 600-nm long-pass filter and 610/20 bandpass filters (Chroma Technology).

Data analysis. All data analysis was performed with custom MATLAB software. Raw cytometry data were filtered to eliminate errors due to uneven sampling time and negative fluorescence readings. Bulk calculations were done on these processed data. To control for cell aggregates, as well as cell size and shape, forward scatter and side scatter (FSC and SSC) data were expressed on orthogonal axes and subpopulations of cells were selected by using circular gates of increasing radii centred on the median FSC and SSC values[11]. Nineteen circular bins were created with radii of 6,000, 9,000, 10^4, 2×10^4, 3×10^4, … , 17×10^4 arbitrary units. Results are shown for data in bin 5, with a radius of 3×10^4. Data were used if at least 5,000 cells were in this bin, but on average between 20,000 and 40,000 cells had FSC and SSC values within this gate. CV was used as a measure of total noise, and intrinsic and extrinsic noise were calculated as described[15] by using GFP and mCherry dual-colour strains (Supplementary Information, Table S2). Student's *t*-tests were used to calculate the level of significance for increases in noise in the *dig1Δ* mutant strains.

FACS and expression dynamics. *pAGA1–YFP dig1Δ* cells were grown to mid-exponential phase. A narrow gate centred on the middle of the fluorescence output distribution was created, and cells with expression levels within this gate were sorted with a Becton Dickinson FACSAria cell sorter. Cells were spun down, resuspended in YPD medium and grown at 30 °C. Aliquots were removed and the fluorescence distributions determined for 30,000 cells with a Becton Dickinson LSR-II flow cytometer. Data were analysed as described above.

Microscopy. Cells were grown overnight to saturation in YPAD. Cultures were diluted back to a D_{600} of 0.1 and grown for 4 h. Microscopy was performed with a DeltaVision deconvolution microscope with Olympus Plan Apo 60× and 100× objectives. *Z*-stacks were taken with 0.3-μm steps. DeltaVision deconvolution software was used to deconvolve and analyse these images. For Ste12–GFP, a 1-s exposure was used; for Nup188–mCherry a 0.5-s exposure was used. For Reb1–GFP a 1.0-s exposure was used. For the Ste12–GFP and Nop7–mCherry co-localization experiments a 0.5-s exposure was used for the fluorescein isothiocyanate channel and a 0.2-s exposure was used for the rhodamine channel.

Quantitative immunoblotting. Cells were grown to exponential phase in YPAD and samples were collected as described[59]. Immunoblotting was performed as described in the Li-COR Odyssey manual with anti-Ste12 (1:1,000 dilution; a gift from Ira Herskowitz), anti-tubulin (1:3,000 dilution; AbCam), anti-rabbit-IR_{800} (1:1,000 dilution) and anti-rat-IR_{680} (1:1,000 dilution).

Growth rate. Cells were grown to exponential phase overnight in YPAD. These cultures were diluted back to $D_{600} = 0.2$ (YM1953, YM2101, YM2315 and YM2643) or $D_{600} = 0.05$ (YM2248, YM3776, YM3777 and YM3778) at $t = 0$, and D_{600} measurements were taken hourly. D_{600} measurements at later time points were normalized to D_{600} at $t = 0$. Best-fit lines were calculated with DeltaGraph 5 graphing software.

Flow cytometry-based cell–cell fusion assay. A *MAT***a** strain (YM2901) containing the amino terminus (residues 1–158) of *eGFP* fused to a leucine zipper dimerization domain[60] was constructed. *MAT*α strains (YM2903, YM3085, YM3086 and YM3087) containing the carboxy terminus (residues 159–240) of *eGFP* fused to a leucine zipper dimerization domain[60] as well as an *mCherry* marker driven by *pTEF2* integrated at the *LYS1* locus were also constructed. Strains were grown overnight to saturation. The cultures were diluted to a D_{600} of 0.07 and collected after outgrowth for 5.5 h. At $t = 0$, each *MAT***a** strain was mixed in tenfold excess with a *MAT*α strain to a final D_{600} of 1.0. A 750-ml aliquot was removed from each mating mix as the zero time point. The rest of the mating culture was dispensed (200 ml per well) into a 96-well Millipore Multi-screen Filter plate and spun in a Beckman centrifuge at 560*g* for 5 min to bind the cells to the filter. The filter plate was placed on a YPAD plate and incubated at 30 °C. Samples were collected in triplicate at the indicated time points. Flow cytometry was conducted as described above in the two-colour assay; between 3,000 and 10,000 cells were analysed for each time point. Data analysis was performed with FlowJo 8.7.1, using quadrants based on the zero time point. Diploids were revealed as $GFP^+/mCherry^+$ cells. To determine mating efficiency, the fraction of diploid cells ($GFP^+/mCherry^+$) divided by the total number of $mCherry^+$ cells ($GFP^{+/-}$) was calculated for each time point in each mating experiment. The mean and s.d. for the three replicates was then calculated for each time point (with the exception of the zero time point).

Pheromone time-course assay. Cells were grown to exponential phase overnight in YPAD and were diluted back to $D_{600} = 0.4$. α-Factor (50 nM) was added. Aliquots of 1 ml were removed at $t = 0$, 15, 30, 60, 90, 120, 150, 180 and 240 min, and fluorescence distributions were measured by flow cytometry. Data were analysed as described above.

ChIP. Dig1–GFP ChIP was performed as described[61,62] with strains YM1731 and YM3747, using an anti-GFP antibody from AbCam (Ab290). α-Factor (5 μM) was added to exponential-phase cultures for 1 h.

Modified ChIP-chip method. An 11-kilobase construct consisting of 240 tandem arrays of Lac operators[63] and an associated *HIS3MX* marker was inserted 331 bp upstream of the *FUS1* ATG in strains containing a mCherry–LacI plasmid (BHM1336 adapted from pJH212, strains YM3587, YM3588 and YM3687). Cultures were prepared for ChIP-chip by growth overnight to saturation in –Ura medium. Cultures were then diluted to $D_{600} = 0.01$ and grown for 4 h in –Ura medium. These cells were again diluted to $D_{600} = 0.01$ in YPAD and collected 4 h later. Chromatin immunoprecipitation was performed as described[61,62]. However, the protein crosslinker ethylene glycolbis (succinimidylsuccinate; EGS) was added to a final concentration of 1.5 mM for 30 min before the addition of formaldehyde. In addition, DNA was lightly sonicated twice in a Diagenode Bioruptor for 5 min on the low setting with 1 s on/0.5 s off pulses. To immunoprecipitate mCherry–LacI, a polyclonal anti-DsRed antibody (Clontech catalogue number 632496) was used at 1:100 dilution. After ChIP, strand displacement amplification and labelling were performed as described to generate DNA probes with incorporated aminoallyl-dUTP[64]. Probes representing mCherry–LacI immunoprecipitates and whole-cell extracts were differentially labelled with Cy fluorescent dyes and hybridized on Agilent yeast whole-genome tiling microarrays (G4491A). Hybridization and array washing were performed as described by Agilent Technologies (Version 9.2). In addition, after the acetonitrile wash, slides were rinsed in Agilent Stabilization and Drying Solution (5185-5979). Microarrays were scanned at 5 μm resolution on a GenePix 4000B scanner (Molecular Devices), using GenePixPro 6.0 software. Microarray analysis was performed with in-house software as described[65]. For each strain (wild type, *dig1Δ* and *dig1Δste12Δ*), data from four arrays were averaged by calculating the geometric mean of the intensities of each probe. Averaged data were then smoothed with a moving-average window over 11 probes and difference maps were constructed by subtracting the $\log_2$ values for each wild-type probe from the corresponding probe in *dig1Δ* and *dig1Δ ste12Δ* data sets. Given the broad peak (due to light sonication) centred on the *FUS1* locus on the left arm of chromosome III, data from this region were removed from further analysis. We extracted 500 bp of sequence upstream of each gene and subdivided these segments into 20 bins, each of which represented 25 bp of sequence. Data from microarray probes were assigned to the appropriate bin based on the genomic coordinate of the centre of a probe. These gene promoter segments were then ordered relative to one another

DOI: 10.1038/ncb2097

on the basis of the median value of all the probes in a segment. The top 5% (269 genes) of differences from each *dig1Δ*–wild-type or *dig1Δste12Δ*–wild-type data set were analysed for enrichment of target genes for 203 transcription factors[21]. Similar results were obtained with 1%, 3% and 10% cutoffs. A list of target genes for the 203 transcription factors was compiled from ChIP-chip data ($P < 0.05$) from ref. 21. Next, we performed hypergeometric testing to determine whether the enrichment of transcription factor target genes in the top 5% of our data sets was statistically significant below a Bonferroni-corrected P value of 0.05 (Supplementary Information, Table S1). We also compiled a list of genes bound by Ste12 or Tec1 in the presence or absence of pheromone ($P < 0.05$)[21]. We analysed our list of genes with the top 5% of differences for an enrichment of these genes and calculated a P value by using hypergeometric testing.

58. Storici, F., Durham, C. L., Gordenin, D. A. & Resnick, M. A. Chromosomal site-specific double-strand breaks are efficiently targeted for repair by oligonucleotides in yeast. *Proc. Natl Acad. Sci. USA* **100,** 14994–14999 (2003).
59. Shock, T. R., Thompson, J., Yates, J. R. III & Madhani, H. D. Hog1 mitogen-activated protein kinase (MAPK) interrupts signal transduction between the Kss1 MAPK and the Tec1 transcription factor to maintain pathway specificity. *Eukaryot. Cell* **8,** 606–616 (2009).
60. Magliery, T. J. *et al.* Detecting protein–protein interactions with a green fluorescent protein fragment reassembly trap: scope and mechanism. *J. Am. Chem. Soc.* **127,** 146–157 (2005).
61. Meneghini, M. D., Wu, M. & Madhani, H. D. Conserved histone variant H2A.Z protects euchromatin from the ectopic spread of silent heterochromatin. *Cell* **112,** 725–736 (2003).
62. Raisner, R. M. *et al.* Histone variant H2A.Z marks the 5′ ends of both active and inactive genes in euchromatin. *Cell* **123,** 233–248 (2005).
63. Lau, I. F. *et al.* Spatial and temporal organization of replicating Escherichia coli chromosomes. *Mol. Microbiol.* **49,** 731–743 (2003).
64. Nobile, C. J. *et al.* Biofilm matrix regulation by *Candida albicans* Zap1. *PLoS Biol.* **7,** e1000133 (2009).
65. Hartley, P. D. & Madhani, H. D. Mechanisms that specify promoter nucleosome location and identity. *Cell* **137,** 445–458 (2009).

nature cell biology

DOI: 10.1038/ncb2097

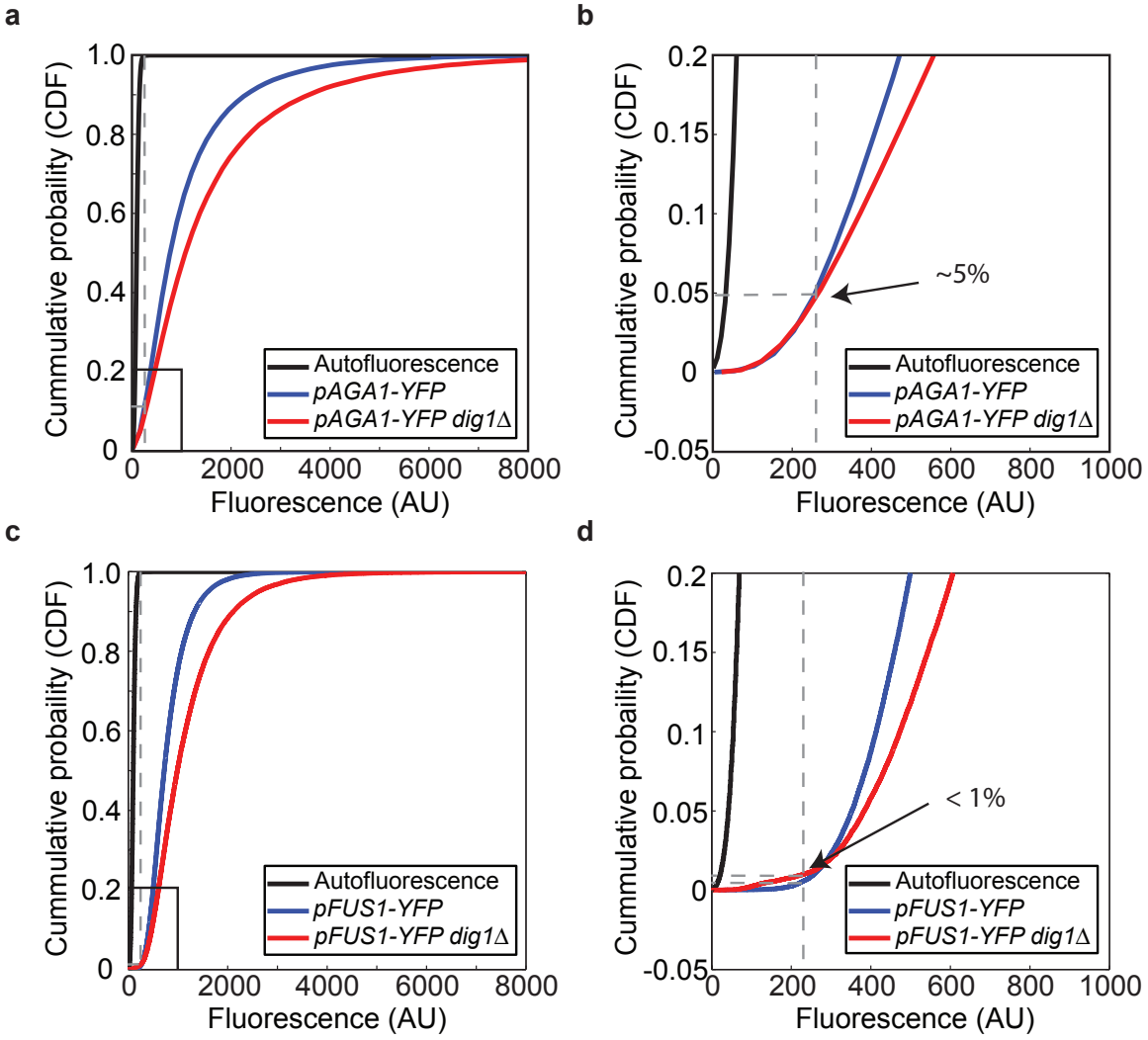

Figure S1 Cumulative probability density functions (CDFs) to measure overlap of fluorescent populations and autofluorescence. **a.** CDFs for non-fluorescent strain (black), *pAGA1-YFP* (blue), *pAGA1 dig1*Δ (red). **b.** Magnification of black box in (**a**). **c.** CDFs for non-fluorescent strain (black), *pFUS1-YFP* (blue) and *pFUS1 dig1*Δ (red). **d.** Magnification of black box in (**c**). **a-d.** The gray dashed line indicates the maximum fluorescence value of non-fluorescent yeast (CDF=1.0). *pAGA1-YFP* wild-type and *dig1*Δ distributions have CDF values of ~0.05 for this fluorescence value (5% of distribution overlaps with autofluorescence). *pFUS1-YFP* wild type and *dig1*Δ distributions have CDF values of <0.01 at this fluorescence value. **a, b, c, d.** CDFs were calculated for the average of measurements on three replicate cultures of a given genotype. At least 5,000, and on average between 20,000 and 40,000, cells were analyzed from each culture.

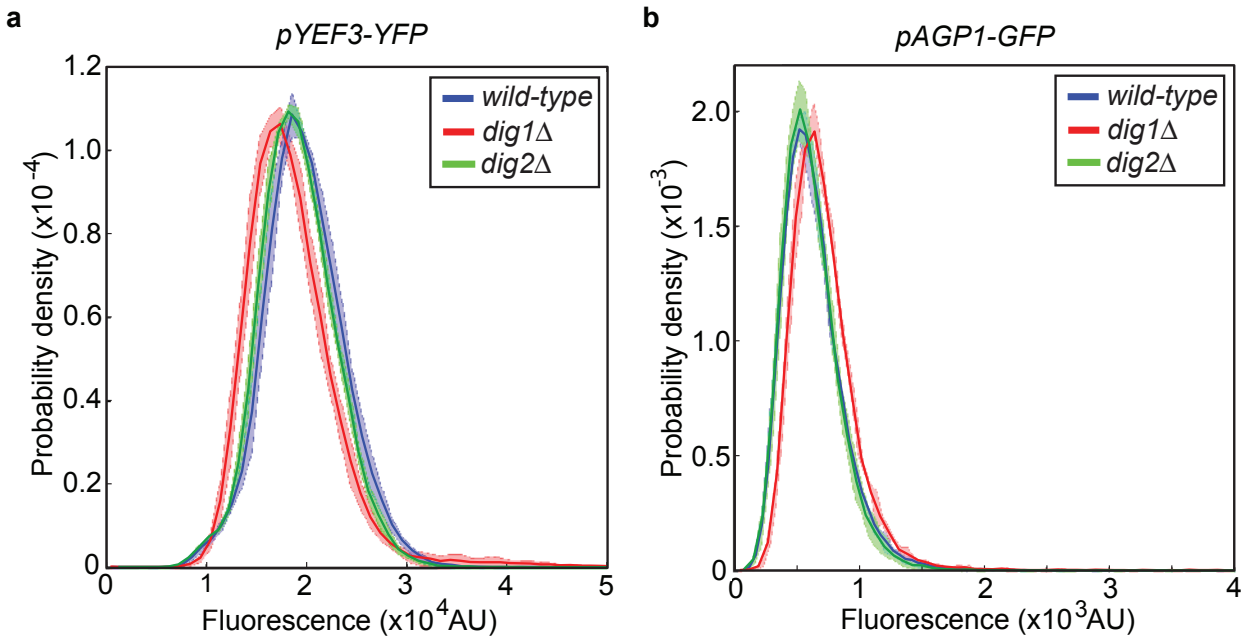

Figure S2 Probability density functions for two Ste12-independent promoters, **a.** *pYEF3* and **b**. *pAGP1*, driving YFP and GFP, respectively. Wild-type is in blue, *dig1*Δ is in red, and *dig2*Δ is in green. Solid line is the mean of measurement of three replicate cultures and the envelope reflects standard deviation. At least 5,000, and on average between 20,000 and 40,000, cells were analyzed from each culture.

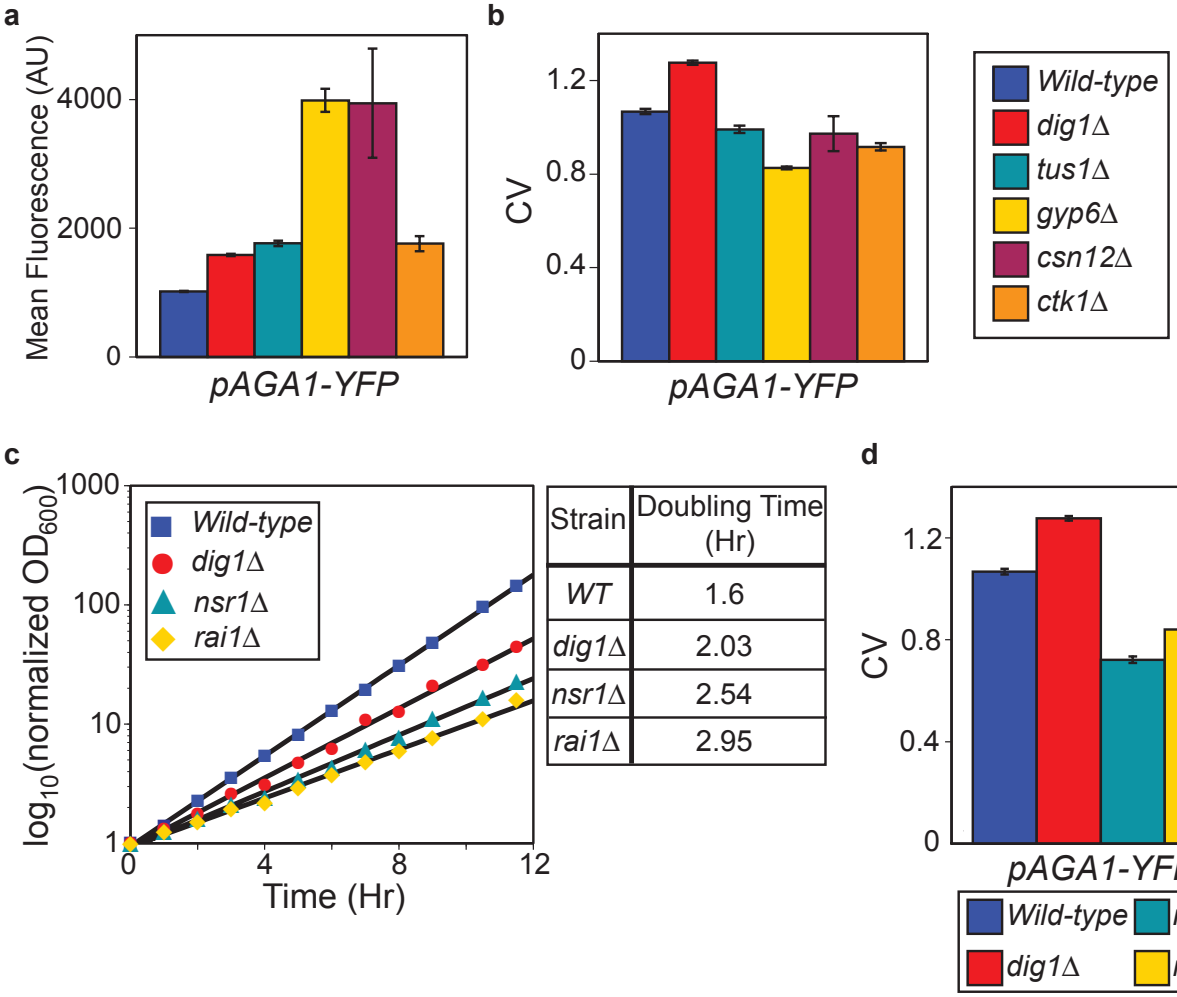

Strain	Doubling Time (Hr)
WT	1.6
*dig1*Δ	2.03
*nsr1*Δ	2.54
*rai1*Δ	2.95

Figure S3 High mean and slow growth are not sufficient to cause increased noise in the output of the pheromone response pathway. **a.** Mean output of *pAGA1-YFP* in wild-type (blue), *dig1*Δ (red), *tus1*Δ (turquoise), *gyp6*Δ (yellow), *csn12*Δ (purple) and *ctk1*Δ (orange). **b.** CV of *pAGA1-YFP* output distributions. Strains are in same colour as in **a. c.** Normalized OD_{600} versus time for wild-type (blue squares), *dig1*Δ (red circles), *nsr1*Δ (turquoise triangles) and *rai1*Δ (yellow diamonds). Doubling times were calculated and are listed in the table. Data shown are representative of two independent experiments. **d.** CV of *pAGA1-YFP* output distributions of same strains as in **c**. **a, b, d.** Error bars represent the standard deviation of measurements performed on three replicate cultures. On average, 100,000 cells were measured for each culture.

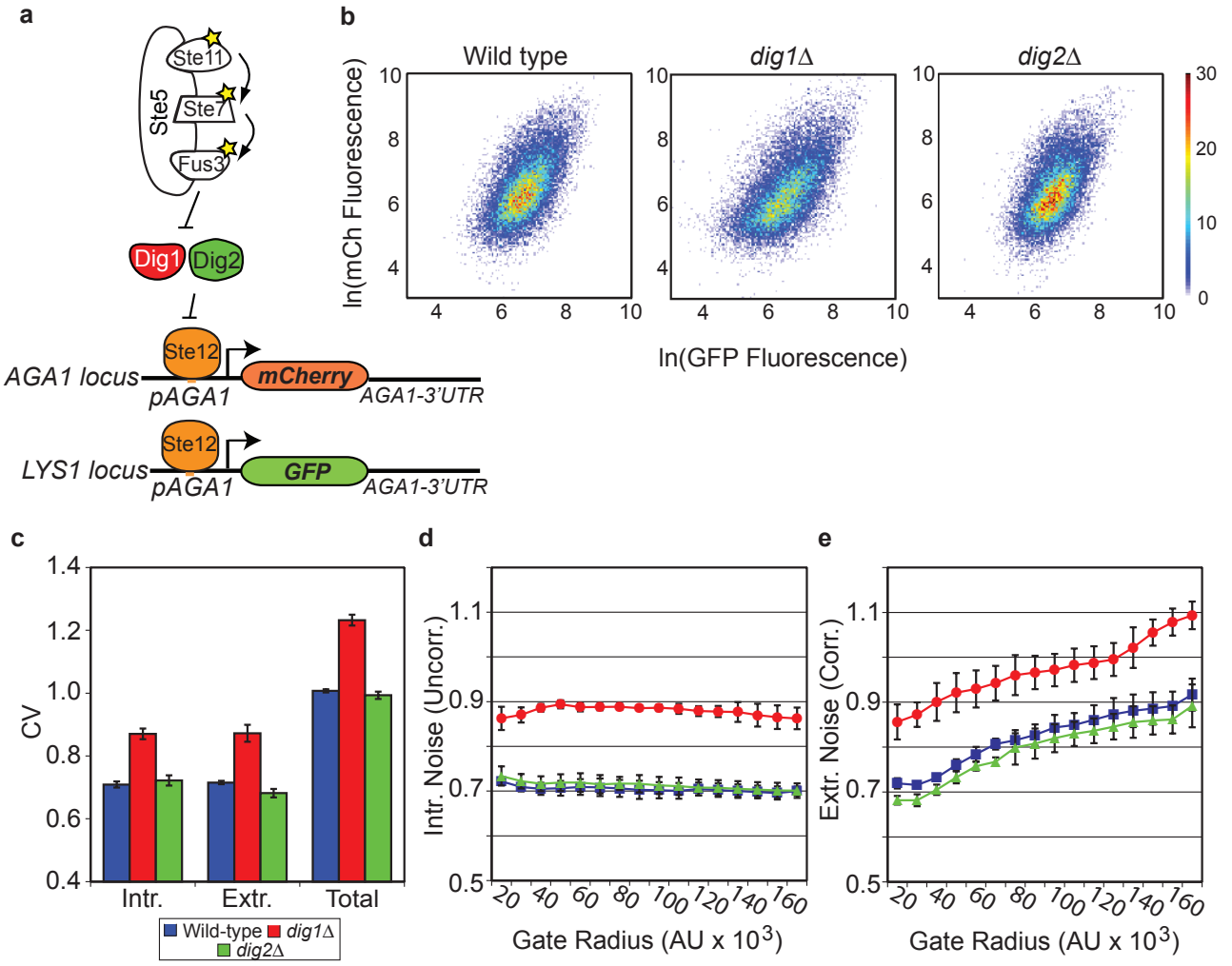

Figure S4 Two-colour experiment with the location of mCherry and GFP reversed. **a.** In this strain, mCherry was inserted in the endogenous *pAGA1* locus while *pAGA1-GFP-AGA1 3'UTR* was inserted in the *LYS1* locus. **b.** Density plots of mCherry vs. GFP fluorescence values for wild-type (left), *dig1*Δ (middle) and *dig2*Δ (right). **c.** CV vs. intrinsic, extrinsic and total noise. Wild-type in blue, *dig1*Δ in red, and *dig2*Δ in green. Total noise was calculated as in **Fig. 2c**. **d,e.** Intrinsic and extrinsic noise vs. gate radius (see Methods for exact gate radii). Wild-type is in blue, *dig1*Δ is in red and *dig2*Δ is in green. **c, d, e.** Error bars represent the standard deviation of measurements performed on three replicate cultures. At least 5,000, and on average between 20,000 and 40,000, cells were analyzed from each culture.

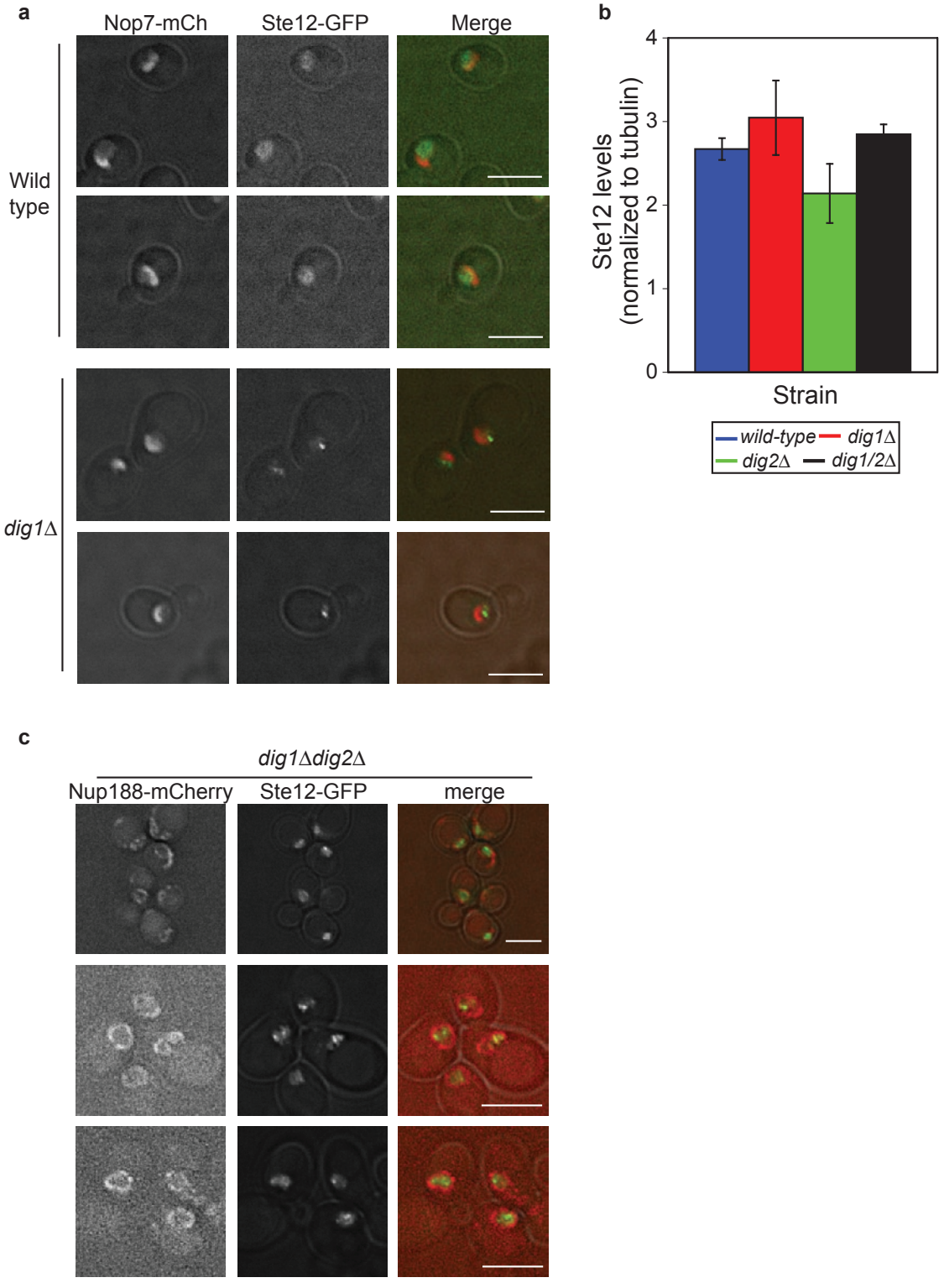

Figure S5 **a.** Ste12-GFP and Nop7-mCherry co-localization in wild-type (top two rows) and *dig1*Δ (bottom two rows) cells. Scale: 5 μm. **b.** Ste12 levels normalized to tubulin in *wild-type* (blue), *dig1*Δ (red), *dig2*Δ (green) and *dig1*Δ*dig2*Δ (black) as measured by quantitative immunoblotting (see Methods). Error bars indicate the standard deviation of measurements performed on three replicate cultures. **c.** Ste12-GFP localization in *STE12-GFP dig1*Δ*dig2*Δ double mutant strains. Scale: 5 μM. **a, b**. Data shown are representative images.

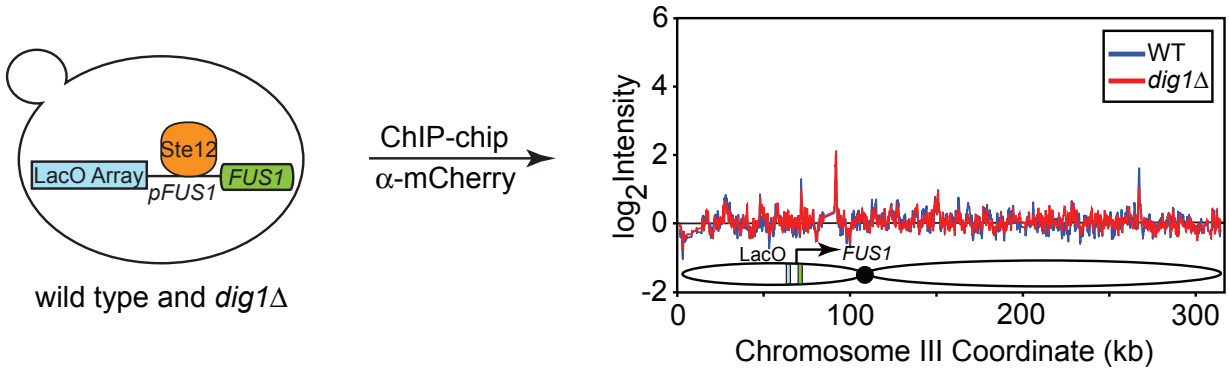

Figure S6 *FUS1* locus does not immunoprecipitate in absence of mCherry-LacI.

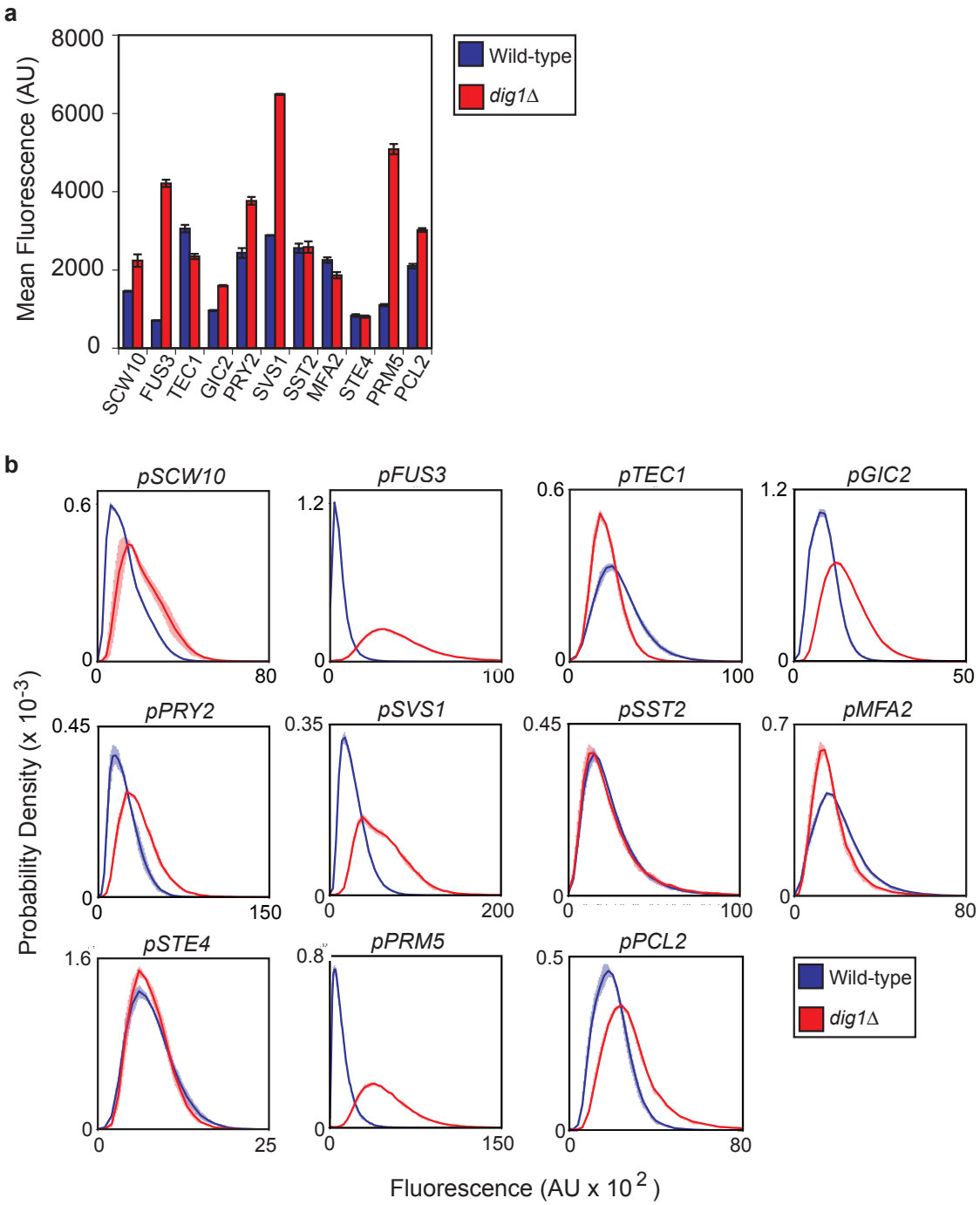

Figure S7 Mean expression and PDFs for 11 reporter strains whose promoters were found to interact with the *FUS1* locus. **a.** Mean fluorescence output for reporter strains in wild-type (blue) and *dig1*Δ (red) cells. Error bars represent the standard deviation of measurements performed on three replicate cultures. **b.** PDFs of output distributions of 11 reporter strains. Wild-type is in blue, *dig1*Δ is in red. The solid line is the average PDF of measurements performed on three replicate cultures and the envelope reflects the standard deviation. **a, b.** On average 100,000 cells were analyzed for each culture.

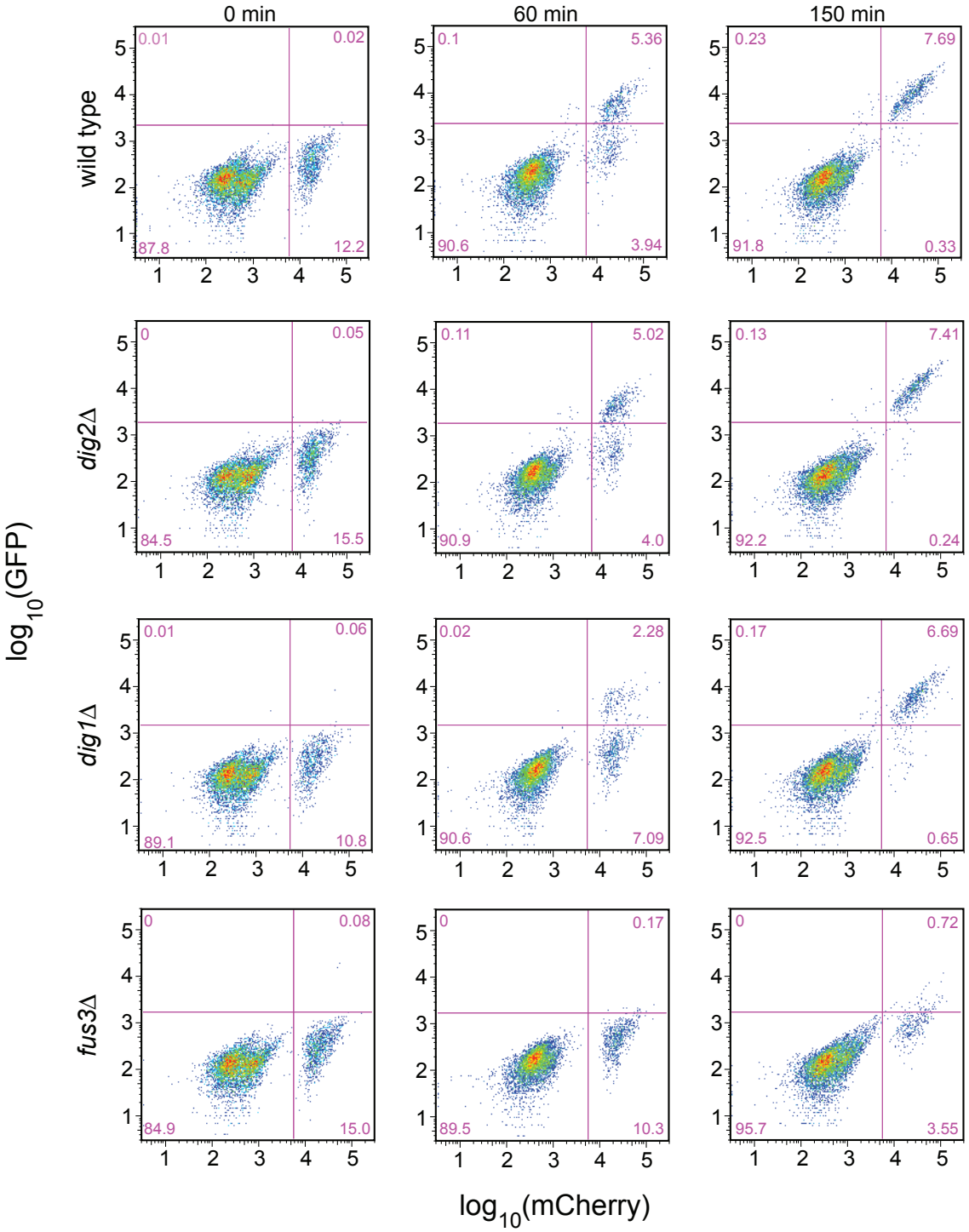

Figure S8 FACS scatter plots of the mating time course assay. GFP vs. mCherry data is plotted for each strain at three time points; 0 min, 60 min and 150 min. The quadrants in each plot separate wild-type unfused *MAT***a** GFP-/mCh- cells, unfused wild-type or mutant *MAT*α GFP-/mCh+ cells and fused GFP+/mCh+ cells. The percentage of cells in each quadrant is listed in pink. Between 3,000 and 10,000 cells were analyzed for each time point.

Table S1: 5% of genes with largest differences in ChIP-chip signals

dig1Δ - wild type
YBL003C/HTA2, YBL008W/HIR1, YBL016W/FUS3, YBL017C/PEP1, YBL026W/LSM2, YBL029W/YBL029W, YBL067C/UBP13, YBL086C/YBL086C, YBR001C/NTH2, YBR040W/FIG1, YBR058C/UBP14, YBR082C/UBC4, YBR083W/TEC1, YBR088C/POL30, YBR095C/RXT2, YBR096W/YBR096W, YBR123C/TFC1, YBR153W/RIB7, YBR168W/PEX32, YBR211C/AME1, YBR233W-A/DAD3, YBR250W/SPO23, YBR291C/CTP1, YCR095W-A/YCR095W-A, YDL013W/SLX5, YDL076C/RXT3, YDL102W/POL3, YDL103C/QRI1, YDL127W/PCL2, YDL133C-A/RPL41B, YDL133W/YDL133W, YDL155W/CLB3, YDL165W/CDC36, YDL166C/FAP7, YDL176W/YDL176W, YDL179W/PCL9, YDR060W/MAK21, YDR100W/TVP15, YDR162C/NBP2, YDR169C-A/YDR169C-A, YDR177W/UBC1, YDR179C/CSN9, YDR179W-A/YDR179W-A, YDR181C/SAS4, YDR204W/COQ4, YDR217C/RAD9, YDR275W/BSC2, YDR309C/GIC2, YDR336W/YDR336W, YDR395W/SXM1, YDR415C/YDR415C, YDR416W/SYF1, YDR439W/LRS4, YDR459C/PFA5, YDR460W/TFB3, YDR464W/SPP41, YDR465C/RMT2, YDR466W/PKH3, YDR468C/TLG1, YDR496C/PUF6, YDR504C/SPG3, YDR507C/GIN4, YDR522C/SPS2, YDR532C/YDR532C, YEL001C/IRC22, YEL042W/GDA1, YER051W/JHD1, YER056C/FCY2, YER062C/HOR2, YER065C/ICL1, YER069W/ARG5,6, YER071C/YER071C, YER072W/VTC1, YER122C/GLO3, YER123W/YER123W, YER139C/RTR1, YER140W/YER140W, YER166W/DNF1, YER168C/CCA1, YFL003C/MSH4, YFL010C/WWM1, YFR002W/NIC96, YFR037C/RSC8, YFR038W/IRC5, YGL001C/ERG26, YGL017W/ATE1, YGL045W/RIM8, YGL067W/NPY1, YGL081W/YGL081W, YGL178W/MPT5, YGR005C/TFG2, YGR006W/PRP18, YGR014W/MSB2, YGR040W/KSS1, YGR071C/YGR071C, YGR074W/SMD1, YGR076C/MRPL25, YGR162W/TIF4631, YGR188C/BUB1, YGR194C/XKS1, YGR201C/YGR201C, YGR236C/SPG1, YGR253C/PUP2, YGR279C/SCW4, YHR016C/YHR016C, YHR017W/YHR017W, YHR082C/KSP1, YHR084W/STE12, YHR086W-A/YHR086W-A, YHR110W/ERP5, YHR122W/YHR122W, YHR128W/FUR1, YHR184W/SSP1, YHR201C/PPX1, YIL053W/RHR2, YIL104C/SHQ1, YIL117C/PRM5, YIL119C/RPI1, YIL123W/SIM1, YIL130W/ASG1, YIL131C/FKH1, YIL139C/REV7, YIL146C/ECM37, YIL147C/SLN1, YIL158W/AIM20, YJL049W/YJL049W, YJL130C/URA2, YJL134W/LCB3, YJL136C/RPS21B, YJL179W/PFD1, YJL180C/ATP12, YJR010C-A/SPC1, YJR010W/MET3, YJR025C/BNA1, YJR154W/YJR154W, YKL042W/SPC42, YKL060C/FBA1, YKL084W/HOT13, YKL096W-A/CWP2, YKL104C/GFA1, YKL138C-A/HSK3, YKL183W/LOT5, YKL207W/LRC3, YKR004C/ECM9, YKR010C/TOF2, YKR011C/YKR011C, YKR013W/PRY2, YKR039W/GAP1, YKR041W/YKR041W, YKR091W/SRL3, YKR095W-A/PCC1, YKR096W/ESL2, YKR103W/NFT1, YLL042C/ATG10, YLL056C/YLL056C, YLR018C/POM34, YLR040C/YLR040C, YLR042C/YLR042C, YLR044C/PDC1, YLR046C/YLR046C, YLR128W/DCN1, YLR129W/DIP2, YLR165C/PUS5, YLR172C/DPH5, YLR173W/YLR173W, YLR209C/PNP1, YLR210W/CLB4, YLR240W/VPS34, YLR248W/RCK2, YLR251W/SYM1, YLR264W/RPS28B, YLR268W/SEC22, YLR271W/YLR271W, YLR305C/STT4, YLR306W/UBC12, YLR309C/IMH1, YLR353W/BUD8, YLR362W/STE11, YLR369W/SSQ1, YLR412C-A/YLR412C-A, YLR421C/RPN13, YLR433C/CNA1, YLR443W/ECM7, YLR452C/SST2, YML018C/YML018C, YML043C/RRN11, YML056C/IMD4, YML092C/PRE8, YMR001C/CDC5, YMR016C/SOK2, YMR038C/CCS1, YMR077C/VPS20, YMR100W/MUB1, YMR115W/MGR3, YMR144W/YMR144W, YMR192W/GYL1, YMR231W/PEP5, YMR234W/RNH1, YMR274C/RCE1, YMR293C/HER2, YMR305C/SCW10, YMR306W/FKS3, YNL024C-A/YNL024C-A, YNL038W/GPI15, YNL051W/COG5, YNL072W/RNH201, YNL087W/TCB2, YNL113W/RPC19, YNL141W/AAH1, YNL145W/MFA2, YNL146C-A/YNL146C-A, YNL154C/YNL154C, YNL163C/RIA1, YNL191W/DUG3, YNL216W/RAP1, YNL246W/VPS75, YNL283C/WSC2, YNL289W/PCL1, YNR010W/CSE2, YOL017W/ESC8, YOL018C/TLG2, YOL023W/IFM1, YOL070C/NBA1, YOL089C/HAL9, YOL159C-A/YOL159C-A, YOR046C/DBP5, YOR060C/YOR060C, YOR081C/TGL5, YOR083W/WHI5, YOR128C/ADE2, YOR137C/SIA1, YOR141C/ARP8, YOR142W/LSC1, YOR156C/NFI1, YOR175C/ALE1, YOR212W/STE4, YOR221C/MCT1, YOR239W/ABP140, YOR246C/YOR246C, YOR247W/SRL1, YOR291W/YOR291W, YPL016W/SWI1, YPL050C/MNN9, YPL054W/LEE1, YPL055C/LGE1, YPL070W/MUK1, YPL071C/YPL071C, YPL117C/IDI1, YPL135W/ISU1, YPL137C/GIP3, YPL141C/YPL141C, YPL163C/SVS1, YPL179W/PPQ1, YPL184C/MRN1, YPL191C/YPL191C, YPL195W/APL5, YPL210C/SRP72, YPL270W/MDL2, YPR035W/GLN1, YPR047W/MSF1, YPR104C/FHL1, YPR137W/RRP9, YPR152C/URN1, YPR153W/YPR153W, YPR155C/NCA2, YPR156C/TPO3, YPR176C/BET2, YPR178W/PRP4, YPR180W/AOS1

dig1Δste12Δ - wild type
YAL064W/YAL064W, YAL067C/SEO1, YAR003W/SWD1, YBL009W/ALK2, YBL010C/YBL010C, YBL097W/BRN1, YBR005W/RCR1, YBR018C/GAL7, YBR019C/GAL10, YBR028C/YBR028C, YBR058C/UBP14, YBR123C/TFC1, YBR129C/OPY1, YBR148W/YSW1, YBR164C/ARL1, YBR166C/TYR1, YBR167C/POP7, YBR168W/PEX32, YBR170C/NPL4, YBR211C/AME1, YBR212W/NGR1, YBR216C/YBP1, YBR217W/ATG12, YBR245C/ISW1, YBR246W/YBR246W, YBR247C/ENP1, YBR254C/TRS20, YBR258C/SHG1, YBR275C/RIF1, YCR018C/SRD1, YCR042C/TAF2, YCR095W-A/YCR095W-A, YDL008W/APC11, YDL036C/PUS9, YDL065C/PEX19, YDL084W/SUB2, YDL102W/POL3, YDL103C/QRI1, YDL146W/LDB17, YDL147W/RPN5, YDL148C/NOP14, YDL156W/CMR1, YDL165W/CDC36, YDL218W/YDL218W, YDR012W/RPL4B, YDR014W/RAD61, YDR026C/YDR026C, YDR060W/MAK21, YDR070C/FMP16, YDR081C/PDC2, YDR140W/MTQ2, YDR160W/SSY1, YDR177W/UBC1, YDR183W/PLP1, YDR184C/ATC1, YDR204W/COQ4, YDR221W/GTB1, YDR244W/PEX5, YDR245W/MNN10, YDR247W/VHS1, YDR273W/DON1, YDR283C/GCN2, YDR315C/IPK1, YDR318W/MCM21, YDR320C/SWA2, YDR321W/ASP1, YDR369C/XRS2, YDR370C/YDR370C, YDR371W/CTS2, YDR374C/YDR374C, YDR414C/ERD1, YDR416W/SYF1, YDR439W/LRS4, YDR468C/TLG1, YDR469W/SDC1, YDR484W/VPS52, YDR503C/LPP1, YDR523C/SPS1, YEL042W/GDA1, YER054C/GIP2, YER107C/GLE2, YER115C/SPR6, YER134C/YER134C, YER139C/RTR1, YER173W/RAD24, YFL004W/VTC2, YFL049W/SWP82, YFL050C/ALR2, YGL016W/KAP122, YGL059W/PKP2, YGL095C/VPS45, YGL171W/ROK1, YGL213C/SKI8, YGL232W/TAN1, YGR001C/AML1, YGR059W/SPR3, YGR169C/PUS6, YGR229C/SMI1, YHL012W/YHL012W, YHL013C/OTU2, YHL046C/PAU13, YHR060W/VMA22, YHR111W/UBA4, YHR129C/ARP1, YHR177W/YHR177W, YHR191C/CTF8, YHR197W/RIX1, YIL084C/SDS3, YIL104C/SHQ1, YIL120W/QDR1, YIL128W/MET18, YIL129C/TAO3, YIL130W/ASG1, YIL131C/FKH1, YIL139C/REV7, YIL146C/ECM37, YJL046W/AIM22, YJL047C/RTT101, YJL049W/YJL049W, YJL085W/EXO70, YJL087C/TRL1, YJL091C/GWT1, YJL097W/PHS1, YJL204C/RCY1, YJL205C/NCE101, YJR010C-A/SPC1, YJR025C/BNA1, YJR107W/YJR107W, YKL001C/MET14, YKL002W/DID4, YKL011C/CCE1, YKL040C/NFU1, YKL090W/CUE2, YKL105C/YKL105C, YKL108W/SLD2, YKL144C/RPC25, YKL166C/TPK3, YKL194C/MST1, YKL206C/ADD66, YKR004C/ECM9, YKR010C/TOF2, YKR051W/YKR051W, YKR084C/HBS1, YKR098C/UBP11, YKR103W/NFT1, YLL042C/ATG10, YLR021W/IRC25, YLR083C/EMP70, YLR102C/APC9, YLR127C/APC2, YLR128W/DCN1, YLR134W/PDC5, YLR165C/PUS5, YLR166C/SEC10, YLR172C/DPH5, YLR173W/YLR173W, YLR188W/MDL1, YLR195C/NMT1, YLR201C/COQ9, YLR207W/HRD3, YLR209C/PNP1, YLR210W/CLB4, YLR234W/TOP3, YLR238W/FAR10, YLR251W/SYM1, YLR284C/ECI1, YLR292C/SEC72, YLR293C/GSP1, YLR305C/STT4, YLR325C/RPL38, YLR329W/REC102, YLR360W/VPS38, YLR361C/DCR2, YLR362W/STE11, YLR398C/SKI2, YLR411W/CTR3, YLR424W/SPP382, YLR440C/SEC39, YLR442C/SIR3, YML017W/PSP2, YML018C/YML018C, YML056C/IMD4, YML108W/YML108W, YML109W/ZDS2, YML110C/COQ5, YMR059W/SEN15, YMR060C/SAM37, YMR061W/RNA14, YMR078C/CTF18, YMR084W/YMR084W, YMR097C/MTG1, YMR106C/YKU80, YMR140W/SIP5, YMR180C/CTL1, YMR233W/TRI1, YMR234W/RNH1, YNL024C-A/YNL024C-A, YNL025C/SSN8, YNL119W/NCS2, YNL121C/TOM70, YNL122C/YNL122C, YNL158W/PGA1, YNL168C/FMP41, YNL191W/DUG3, YNL246W/VPS75, YNL249C/MPA43, YNL259C/ATX1, YNL260C/YNL260C, YNL265C/IST1, YNL308C/KRI1, YNR010W/CSE2, YNR048W/YNR048W, YNR055C/HOL1, YNR061C/YNR061C, YNR063W/YNR063W, YOL017W/ESC8, YOL018C/TLG2, YOL023W/IFM1, YOL024W/YOL024W, YOL102C/TPT1, YOL137W/BSC6, YOR046C/DBP5, YOR068C/VAM10, YOR115C/TRS33, YOR116C/RPO31, YOR150W/MRPL23, YOR156C/NFI1, YOR177C/MPC54, YOR188W/MSB1, YOR212W/STE4, YOR214C/YOR214C, YOR239W/ABP140, YOR270C/VPH1, YOR280C/FSH3, YOR281C/PLP2, YOR284W/HUA2, YOR287C/YOR287C, YOR350C/MNE1, YOR356W/YOR356W, YOR363C/PIP2, YPL027W/SMA1, YPL054W/LEE1, YPL092W/SSU1, YPL109C/YPL109C, YPL119C/DBP1, YPL125W/KAP120, YPL167C/REV3, YPL168W/YPL168W, YPL169C/MEX67, YPL180W/TCO89, YPL184C/MRN1, YPL187W/MF(ALPHA)1, YPL195W/APL5, YPL225W/YPL225W, YPL232W/SSO1, YPL266W/DIM1, YPR009W/SUT2, YPR027C/YPR027C, YPR057W/BRR1, YPR068C/HOS1, YPR073C/LTP1, YPR084W/YPR084W, YPR117W/YPR117W, YPR122W/AXL1, YPR176C/BET2, YPR178W/PRP4, YPR187W/RPO26, YPR188C/MLC2, YPR189W/SKI3,

Table S2: List of strains used in this study

Strain #	Genotype	Source
YM1731	*MAT***a** *ura3Δ0 his3Δ1 leu2Δ0 lys2Δ0 met15Δ0*	
YM1953	*MAT***a** *ura3Δ0 his3Δ1 leu2Δ0 lys2Δ0 met15Δ0 bar1::NatMX4*	This study
YM1968	YM1953 *aga1::YFP*	This study
YM2091	YM1953 *fus1::YFP*	This study
YM2100	YM2091 *dig1::KanMX4*	This study
YM2101	YM1953 *dig1::KanMX6*	This study
YM2102	YM2101 *dig2::HisMX6*	This study
YM2105	YM1968 *dig1::KanMX4*	This study
YM2109	YM2105 *dig2::HisMX6*	This study
YM2112	YM2100 *dig2::HisMX6*	This study
YM2248	*MAT***a** *can1::pSTE2-S.p.HIS5 lyp1Δ his3Δ1 leu2Δ0 ura3Δ0 met15Δ0 LYS2+ bar1::NatMX4 hygMX-pAGA1-YFP-3'AGA1-C.g.LEU2*	This study
YM2315	YM1953 *dig2::HisMX6*	This study
YM2636	*MAT***a** *ura3Δ0 his3Δ1 leu2Δ0 lys2Δ0 bar1::NatMX4 aga1::eGFP lys1::pAGA1-mCherry-3'UTR AGA1*	This study
YM2637	*MAT***a** *ura3Δ0 his3Δ1 leu2Δ0 lys2Δ0 bar1::NatMX4 aga1::mCherry lys1::pAGA1-eGFP-3'UTR AGA1*	This study
YM2643	YM1953 *dig1::KanMX6 ste12::His3MX6*	This study
YM2871	YM2636 *dig1::KanMX6*	This study
YM2872	YM2637 *dig2::KanMX6*	This study
YM2875	YM2637 *dig1::KanMX6*	This study
YM2876	YM2636 *dig2::KanMX6*	This study
YM2901	*MAT***a** *ura3Δ0 his3Δ1 leu2Δ0 lys2Δ0 eGFP(aa1-158)-TRP1-NatMX4* (eGFP fragment from W. Lim)	This study
YM2903	*MATα ura3Δ0 his3Δ1 leu2Δ0 lys2Δ0 eGFP(aa159-240)-LEU2 lys1::KanMX6-pTEF2-mCherry* (eGFP fragment from W. Lim)	This study
YM2910	*MAT***a** *ura3Δ0 his3Δ1 leu2Δ0 met15Δ0 STE12-eGFP-HIS3MX6 NUP188-mCherry-URA3MX*	This study
YM3085	YM2903 *fus3::NatMX4*	This study
YM3086	YM2903 *dig2::NatMX4*	This study
YM3087	YM2903 *dig1::NatMX4*	This study
YM3099	YM1968 *dig2::HIS3MX6*	This study
YM3101	YM2091 *dig2::HIS3MX6*	This study
YM3102	YM2910 *dig1::KanMX6*	This study
YM3103	YM2910 *dig2::KanMX6*	This study
YM3104	YM3102 *dig2::NatMX4*	This study
YM3105	YM1968 *pSTE12::pEAF3* (-530bp to ATG removed upstream of *STE12* and replaced with intergenic region upstream of *EAF3*)	This study
YM3106	YM1968 *pSTE12::pTAF4* (-530bp to ATG removed upstream of *STE12* and replaced with intergenic region upstream of *TAF4*)	This study
YM3108	YM3105 *dig1::KanMX6*	This study
YM3109	YM3105 *dig2::KanMX6*	This study
YM3110	YM3106 *dig1::KanMX6*	This study
YM3111	YM3106 *dig2::KanMX6*	This study
YM3132	YM2871 *dig2::HIS3MX6*	This study
YM3133	YM2875 *dig2::HIS3MX6*	This study
YM3545	*MAT***a** *ura3Δ0 his3Δ1 leu2Δ0 lys2Δ0 met15Δ0 bar1::NatMX4 lys1::pYEF3-YFP-3'UTR YEF3*	This study
YM3546	YM3545 *dig1::KanMX6*	This study
YM3547	YM3545 *dig2::HIS3MX6*	This study
YM3550	YM1953 *pmp1::GFP-HIS3MX*	This study
YM3552	YM1953 *agp1::GFP-HIS3MX*	This study
YM3587	*MAT***a** *ura3Δ0 his3Δ1 leu2Δ0 met15Δ0 STE12-eGFP-Hyg3MX LacO-HIS3MX6-pFUS1 pRS316-mCherry-LacI* (LacO from pLAU43 and LacI from JH2129)	This study
YM3588	YM3587 *dig1::KanMX6*	This study
YM3593	YM3550 *dig1::KanMX*	This study
YM3594	YM3550 *dig2::KanMX6*	This study

YM3595	YM3552 *dig1::KanMX6*	This study
YM3596	YM3552 *dig2::KanMX6*	This study
YM3612	YM3593 *dig2::Hyg3MX*	This study
YM3628	YM3550 *lys1::pPMP1-mCherry-URA3MX*	This study
YM3629	YM3628 *dig1::KanMX6*	This study
YM3630	YM3628 *dig2::KanMX6*	This study
YM3631	YM3629 *dig2::Hyg3MX6*	This study
YM3639	*MAT***a** *ura3Δ0 his3Δ1 leu2Δ0 met15Δ0 LacO-HIS3MX6-pFUS1* (LacO from pLAU43)	This study
YM3640	*MAT***a** *ura3Δ0 his3Δ1 leu2Δ0 met15Δ0 LacO-HIS3MX6-pFUS1 dig1::KanMX6* (LacO from pLAU43)	This study
YM3687	*MAT***a** *ura3Δ0 his3Δ1 leu2Δ0 met15Δ0 ste12::NatMX4 LacO-HIS3MX6-pFUS1 dig1::KanMX6 pRS316-mCherry-LacI* (LacO from pLAU43 and LacI from JH2129)	This study
YM3722	*MAT***a** *ura3Δ0 his3Δ1 leu2Δ0 met15Δ0 REB1-eGFP-HIS3MX6 NUP188-mCherry-URA3MX*	This study
YM3723	YM3722 *dig1::KanMX6*	This study
YM3724	YM3722 *dig2::KanMX6*	This study
YM3747	*MAT***a** *ura3Δ0 his3Δ1 leu2Δ0 met15Δ0 DIG1-eGFP-HIS3MX6 NUP188-mCherry-URA3MX*	This study
YM3760	*MAT***a** *ura3Δ0 his3Δ1 leu2Δ0 met15Δ0 lys1::pSST2-YFP-3'SST2*	This study
YM3762	*MAT***a** *ura3Δ0 his3Δ1 leu2Δ0 met15Δ0 lys1::pTEC1-YFP-3'TEC1*	This study
YM3763	*MAT***a** *ura3Δ0 his3Δ1 leu2Δ0 met15Δ0 lys1::pGIC2-YFP-3'GIC2*	This study
YM3764	*MAT***a** *ura3Δ0 his3Δ1 leu2Δ0 met15Δ0 lys1::pFUS3-YFP-3'FUS3*	This study
YM3766	*MAT***a** *ura3Δ0 his3Δ1 leu2Δ0 met15Δ0 lys1::pPRY2-YFP-3'PRY2*	This study
YM3767	*MAT***a** *ura3Δ0 his3Δ1 leu2Δ0 met15Δ0 lys1::pSVS1-YFP-3'SVS1*	This study
YM3769	*MAT***a** *ura3Δ0 his3Δ1 leu2Δ0 met15Δ0 lys1::pSTE4-YFP-3'STE4*	This study
YM3770	*MAT***a** *ura3Δ0 his3Δ1 leu2Δ0 met15Δ0 lys1::pPRM5-YFP-3'PRM5*	This study
YM3771	*MAT***a** *ura3Δ0 his3Δ1 leu2Δ0 met15Δ0 lys1::pPCL2-YFP-3'PCL2*	This study
YM3772	*MAT***a** *ura3Δ0 his3Δ1 leu2Δ0 met15Δ0 lys1::pPCL1-YFP-3'PCL1*	This study
YM3773	*MAT***a** *ura3Δ0 his3Δ1 leu2Δ0 met15Δ0 lys1::pMFA2-YFP-3'MFA2*	This study
YM3774	*MAT***a** *ura3Δ0 his3Δ1 leu2Δ0 met15Δ0 STE12-eGFP-HIS3MX6 NOP7-mCherry-URA3MX*	This study
YM3775	*MAT***a** *ura3Δ0 his3Δ1 leu2Δ0 met15Δ0 STE12-eGFP-HIS3MX6 NOP7-mCherry-URA3MX dig1::KanMX6*	This study
YM3776	*MAT***a** *can1::pSTE2-S.p.HIS5 lyp1Δ his3Δ1 leu2Δ0 ura3Δ0 met15Δ0 LYS2+ bar1::NatMX4 hygMX-pAGA1-YFP-3'AGA1-C.g.LEU2 dig1::KanMX6*	This study
YM3777	*MAT***a** *can1::pSTE2-S.p.HIS5 lyp1Δ his3Δ1 leu2Δ0 ura3Δ0 met15Δ0 LYS2+ bar1::NatMX4 hygMX-pAGA1-YFP-3'AGA1-C.g.LEU2 nsr1::KanMX6*	This study
YM3778	*MAT***a** *can1::pSTE2-S.p.HIS5 lyp1Δ his3Δ1 leu2Δ0 ura3Δ0 met15Δ0 LYS2+ bar1::NatMX4 hygMX-pAGA1-YFP-3'AGA1-C.g.LEU2 rai1::KanMX6*	This study
YM3779	*MAT***a** *can1::pSTE2-S.p.HIS5 lyp1Δ his3Δ1 leu2Δ0 ura3Δ0 met15Δ0 LYS2+ bar1::NatMX4 hygMX-pAGA1-YFP-3'AGA1-C.g.LEU2 tus1::KanMX6*	This study
YM3780	*MAT***a** *can1::pSTE2-S.p.HIS5 lyp1Δ his3Δ1 leu2Δ0 ura3Δ0 met15Δ0 LYS2+ bar1::NatMX4 hygMX-pAGA1-YFP-3'AGA1-C.g.LEU2 gyp6::KanMX6*	This study
YM3781	*MAT***a** *can1::pSTE2-S.p.HIS5 lyp1Δ his3Δ1 leu2Δ0 ura3Δ0 met15Δ0 LYS2+ bar1::NatMX4 hygMX-pAGA1-YFP-3'AGA1-C.g.LEU2 csn12::KanMX6*	This study
YM3782	*MAT***a** *can1::pSTE2-S.p.HIS5 lyp1Δ his3Δ1 leu2Δ0 ura3Δ0 met15Δ0 LYS2+ bar1::NatMX4 hygMX-pAGA1-YFP-3'AGA1-C.g.LEU2 ctk1::KanMX6*	This study
YM3804	*MAT***a** *ura3Δ0 his3Δ1 leu2Δ0 met15Δ0 lys1::pSST2-YFP-3'SST2 dig1:::KanMX6*	This study
YM3805	*MAT***a** *ura3Δ0 his3Δ1 leu2Δ0 met15Δ0 lys1::pTEC1-YFP-3'TEC1 dig1::HIS3MX6*	This study
YM3806	*MAT***a** *ura3Δ0 his3Δ1 leu2Δ0 met15Δ0 lys1::pGIC2-YFP-3'GIC2 dig1::KanMX6*	This study
YM3807	*MAT***a** *ura3Δ0 his3Δ1 leu2Δ0 met15Δ0 lys1::pFUS3-YFP-3'FUS3 dig1::HIS3MX6*	This study
YM3808	*MAT***a** *ura3Δ0 his3Δ1 leu2Δ0 met15Δ0 lys1::pPRY2-YFP-3'PRY2 dig1::KanMX6*	This study
YM3809	*MAT***a** *ura3Δ0 his3Δ1 leu2Δ0 met15Δ0 lys1::pSVS1-YFP-3'SVS1 dig1::KanMX6*	This study
YM3810	*MAT***a** *ura3Δ0 his3Δ1 leu2Δ0 met15Δ0 lys1::pSTE4-YFP-3'STE4 dig1::HIS3MX6*	This study
YM3811	*MAT***a** *ura3Δ0 his3Δ1 leu2Δ0 met15Δ0 lys1::pPRM5-YFP-3'PRM5 dig1::KanMX6*	This study
YM3812	*MAT***a** *ura3Δ0 his3Δ1 leu2Δ0 met15Δ0 lys1::pPCL2-YFP-3'PCL2 dig1::KanMX6*	This study
YM3813	*MAT***a** *ura3Δ0 his3Δ1 leu2Δ0 met15Δ0 lys1::pPCL1-YFP-3'PCL1 dig1::HIS3MX6*	This study
YM3814	*MAT***a** *ura3Δ0 his3Δ1 leu2Δ0 met15Δ0 lys1::pMFA2-YFP-3'MFA2 dig1::KanMX6*	This study